Pure Appl. Chem., Vol. 77, No. 4, pp. 683–737, 2005.
DOI: 10.1351/pac200577040683

INTERNATIONAL UNION OF PURE AND APPLIED CHEMISTRY

INORGANIC CHEMISTRY DIVISION
COMMISSION ON HIGH TEMPERATURE AND SOLID STATE CHEMISTRY*

HIGH-TEMPERATURE MASS SPECTROMETRY: INSTRUMENTAL TECHNIQUES, IONIZATION CROSS-SECTIONS, PRESSURE MEASUREMENTS, AND THERMODYNAMIC DATA

(IUPAC Technical Report)

Prepared for publication by
JEAN DROWART[1,‡], CHRISTIAN CHATILLON[2], JOHN HASTIE[3], AND DAVID BONNELL[3]

[1]Department of Chemistry, Vrije Universiteit Brussel, Pleinlaan 2, B-1050 Brussels, Belgium; [2]Laboratoire de Thermodynamique et Physico-Chimie Métallurgiques (Associé au CNRS UMR 5614), ENSEEG BP 75 38402-Saint Martin d' Hères, France; [3]National Institute of Standards and Technology, Gaithersburg, MD 20899-8522, USA

*Membership of Commission II.3 during achievement of this work (1982–2001) was as follows:

M. A. Alario Franco (Spain); the late C. B. Alcock (Canada); O. L. Alves (Brazil); A.-M. Anthony (France); M. B. Badri (Malaysia); G. Balducci (Italy); E. J. Baran (Argentina); J.-F. Baumard (France); G. Bayer (Switzerland); H.-P. Boehm (Germany); R. J. Brook (Germany); J. O. Carlsson (Sweden); A. V. Chadwick (UK); C. B. J. Chatillon (France); J.-H. Choy (Korea); J. B. Clark (South Africa); J. Corish (Chairman, 1991–1995; Secretary, 1987–1991; Ireland); F. M. Costa (Portugal); J.-P. Coutures (France); G. De Maria (Italy); D. de Waal (South Africa); M. Drabik (Slovak Republic); J. D. Drowart (Belgium); P. Echegut (France); J. G. Edwards (USA); M. S. E. El-Sewefy (Egypt); P. Ettmayer (Austria); the late E. Fitzer (Germany); the late P. W. Gilles (Secretary, 1981–1987; USA); J. Gopalakrishnan (India); L. N. Gorokhov (Russia); G. P. Grieveson (UK); the late L. V. Gurvich (USSR/Russia); F. Hanic (Slovak Republic); J. W. Hastie (USA); H. Hausner (Germany); M. G. Hocking (UK); D. Holland (UK); B. G. Hyde (Australia); M. Jafelicci, Jr. (Brazil); L. Kihlborg (Sweden); C. H. Kim (Korea); M. Kizilyalli (Turkey); R. Kniep (Germany); the late D. Kolar (Secretary, 1996–1999; Slovenia); K. L. Komarek (Chairman, 1981–1985; Austria); K. Koumoto (Japan); M. Leskela (Finland); M. H. Lewis (UK); C. M. Lieber (USA); J. Livage (France); B. Lux (Austria); K. J. D. MacKenzie (New Zealand); the late A. Magnéli (Sweden); C. K. Mathews (India); J. Matousek (Czechoslovakia/Czech Republic); H. J. Matzke (Germany); E. R. McCartney (Australia); R. Metselaar (Chairman, 1985–1991; Netherlands); J. Mintmire (USA); A. Mocellin (Switzerland); S. Mrowec (Poland); W.-L. Ng (Malaysia); M. Nygren (Sweden); R. W. Ohse (Germany); P. Peshev (Bulgaria); G. Petzow (Germany); M. H. Rand (UK); M. M. Ristic (Yugoslavia); G. M. Rosenblatt (Chairman, 1996–1997; Secretary, 1994–1995; USA); P. Saha (India); T. Saito (Japan); T. Sata (Japan); R. Sersale (Italy); F. Solymosi (Hungary); S. Somiya (Japan); K. E. Spear (Chairman, 1998–1999; USA); G. V. Subba Rao (India); A. P. B. Sinha (India); M. Thackeray (South Africa); L. Tichý (Czech Republic); R. J. D. Tilley (UK); G. Van Tendeloo (Belgium); R. Vernerkar (India); H. Verweij (USA); G. F. Voronin (Russia); N. E. Walsö de Reca (Argentina); W. L. Worrell (USA); D.-S. Yan (China); H. Yanagida (Japan); T.-S. Yen (China); J. J. Ziólkowski (Poland).

‡Corresponding author

High-temperature mass spectrometry: Instrumental techniques, ionization cross-sections, pressure measurements, and thermodynamic data

(IUPAC Technical Report)

Abstract: An assessment of high-temperature mass spectrometry and of sources of inaccuracy is made. Experimental, calculated, and estimated cross-sections for ionization of atoms and inorganic molecules typically present in high-temperature vapors are summarized. Experimental cross-sections determined for some 56 atoms are generally close to theoretically calculated values, especially when excitation–autoionization is taken into account. Absolute or relative cross-sections for formation of parent ions were measured for ca. 100 molecules. These include homonuclear diatomic and polyatomic molecules, oxides, chalcogenides, halides, and hydroxides. Additivity of atomic cross-sections supplemented by empirical corrections provides fair estimates of molecular cross-sections. Causes of uncertainty are differences in interatomic distances and in shapes of potential energy curves (surfaces) of neutral molecules and of molecular ions and tendency toward dissociative ionization in certain types of molecules. Various mass spectrometric procedures are described that render the accuracy of measured thermodynamic properties of materials largely independent of ionization cross-sections. This accuracy is comparable with that of other techniques applicable under the conditions of interest, but often only the mass spectrometric procedure is appropriate at high temperatures.

Keywords: mass spectrometry; high-temperature mass spectrometry; ionization cross-sections; cross-sections; dissociative ionization; ionization; high temperature; Division II.

CONTENTS

1. INTRODUCTION

Determination of thermodynamic properties at high temperatures for condensed phases and for gaseous or vapor species by mass spectrometric (MS) study of vaporization processes [1,2] has been performed for 50 years. During this period, a number of review papers have appeared describing instruments and experimental procedures in high-temperature mass spectrometry (HTMS) [3–28]. Synopses of the results have also been presented [3–6,8–10,14,17,18,20–28]. Data obtained by this technique for individual compounds, whether gaseous or in the condensed phase, are incorporated in tabulations of dissociation energies [29–38], of thermodynamic properties [32–38], and of ionization potentials [30,39,40].

A key aspect of the method is the conversion of primary mass spectral ion intensity data for individual species at specified temperatures to absolute or relative partial pressures. The purpose of the present report is to assess the accuracy and precision of pressures obtained from MS measurements. Attention is paid to the influence of ionization cross-sections and of other factors on such data.

2. PRINCIPLES OF THE METHOD

The basic principles of HTMS methods are:

- to cause a condensed-phase system to vaporize at a known temperature, in general at conditions close to equilibrium, under vacuum, or in the presence of an externally imposed and controlled pressure;
- to form a properly collimated molecular beam in which the flux of each vapor species can be related to the partial pressure of that atom or molecule;
- to submit the atoms and molecules in the beam to ionization in the source of a mass spectrometer;
- to determine the mass-to-charge ratio for each atomic and molecular ion formed, and to measure the mass-selected intensities as a function of a sufficient number of parameters to reconstruct the physical processes relating the ions to the gaseous species they were formed from;

- by appropriate calibration, to convert the ion intensities for individual species or their ratios into absolute or relative partial pressures in the vapor under investigation; and
- to insert the partial pressures obtained into established thermodynamic formulae relating Gibbs energies, enthalpies, entropies, or free energy functions, and to determine the variation of these properties with temperature and/or composition.

When the Knudsen effusion mass spectrometric (KMS) method is used to study molecular beams, calculation of the steady-state number density in the latter and application of the Beer–Lambert law to ionization at low number density provide [4,16]:

$$p_j = I^+_{jk} T / S_{jk} \tag{1}$$

p_j is the partial pressure at temperature T of species j in the gas under analysis, I^+_{jk} the intensity recorded for the ion k formed from moiety j, and S_{jk} the sensitivity of the instrumental assembly and ionization process. S_{jk} is itself proportional to an instrument factor g that is assumed to be independent of j. S_{jk} is also proportional to ε_k, the extraction coefficient from the ionization source, τ_k the transmission of the mass analyzer, γ_k the detection coefficient of the ion k, and f_k the isotopic abundance fraction [41,42] of ion k. S_{jk} in particular further depends on the partial ionization cross-section $\sigma_{jk}(E)$ of the neutral species j for forming the ion k at an ionizing electron energy E. As will be discussed later, σ is a function of E and sometimes of T. We will also discuss the relationship between and the use of partial (σ_{jk}) and total (σ_j) ionization cross-sections.

In summary,

$$S_{jk} = g\varepsilon_k \tau_k \sigma_{jk}(E,T) \gamma_k f_k \tag{2}$$

When high-pressure or supersonic molecular beam sampling methods are used [15,19,23], relations 1 and 2 connecting the observed ion intensity and the original partial pressure of the species remain essentially valid. However, the instrument factor g then becomes a function of the total pressure, requiring special treatment (see Section 4.5).

3. ANALYSIS OF FACTORS DETERMINING ACCURACY

Mass spectrometric studies in high-temperature chemistry, aimed at the determination of thermodynamic properties for condensed phases and for gaseous molecules, mostly make use of Knudsen effusion (see, e.g., [1–14,17,20,21,24–28]) or of vapor transport supersonic molecular beam sampling methods (see, e.g., [15,19]) to generate the molecular beam that is to be analyzed with respect to the nature and the pressure of the gaseous chemical entities present in the cell containing the sample.

Four groups of factors that influence accuracy, introduced and discussed separately as far as possible, are: instrumental, physical, chemical, and physicochemical, thermodynamic. Distinction is further made between avoidable or detectable systematic errors connected with the limitations of experimental assemblies, random uncertainties, and systematic uncertainties that are at present either unknown or difficult to correct for.

Instrumental factors include:

- the design of the Knudsen cell assembly or, in the transport method, of the container-sampling probe assembly;
- the mode of heating these devices;
- the measurement of temperature;
- the mode of forming the molecular beam;
- the spatial extent and the orientation of the beam with respect to the ion source of the mass spectrometer;
- the type of mass spectrometer;

- the ion detector/collector; and
- the quality of the vacuum achieved in the assembly.

Instrumental factors also include the geometry of the ion source, the construction of the filament(s) or cathode assembly, the ionizing current regulation, and various parameters involved in operating the ion source.

Physical factors are mainly related to the need to ionize the species in order to achieve their identification and to measure their partial pressure. It is, hence, necessary to reconstruct the nature of the ionization processes that led from the neutral precursor to be identified to the ion(s) actually observed. The physical factors, as defined here, include cross-sections for ionization, which are discussed separately. The evolution in time of the ion between its formation and the moment it is actually mass analyzed, should also be considered.

Chemical and physicochemical factors include:

- the purity of the substances under investigation;
- the possible modification of the activity of pure substances as a result of their interaction with the container or other substances with which they coexist;
- the degree of establishment of mutual equilibrium between these substances as well as with the gas phase;
- the modification of partial pressures by the sampling process; and
- the phase relationships at each time during the experiment.

Thermodynamic factors include the thermal data for the relevant condensed and gaseous phases. Since thermodynamic functions for gaseous atoms and molecules are calculated with statistical mechanical formulae, the accuracy of spectroscopically determined, quantum-chemically calculated, and especially empirically estimated molecular constants also requires consideration. Physicochemical and thermodynamic factors are in fact the same in the procedures analyzed here and in other methods of pressure determination.

4. INSTRUMENTAL FACTORS

4.1 Temperature measurement

When the temperature of the cell and/or the reactor is measured with a thermocouple, use of sheathed wires is recommended to avoid deterioration or contamination of the thermocouple materials by chemical attack from effusing vapors. Use of uninterrupted wires down to a 0 ºC thermostatic bath or a temperature-compensated cold junction is important. To avoid excessive heat leak by the presence of the thermocouple, several cm of the thermocouple wire near the hot junction should be coiled up in a region near the cell isothermal with the sample. To ensure good thermal equilibration between the cell and the thermocouple, it should be solidly and intimately attached, typically screw-tightened, welded, or swaged. Use of these procedures is necessary to ascertain reproducibility of temperature measurements within 0.5 K.

In optical pyrometric temperature determinations, the interior of the effusion cell often may serve as a black-body cavity. Alternately, cylindrical holes with length/diameter ratios greater than 8 [43] should be drilled in the cell body as close as possible to the sample surface. The absorbance of the window and of other optical elements should be carefully determined to allow calculation of the true thermodynamic temperature from the measured apparent value. Intercepting the molecular beam with movable devices (“shutters”, “flags”, “beam stops” [44]) is essential to minimize vapor deposition on viewports, which should be regularly cleaned and recalibrated.

The sample or its evaporating surface should be as close as possible to the region where the temperature is actually measured in any of the ways mentioned, unless it is established that the entire oven

assembly is isothermal. This point will be discussed further in connection with cell shape and furnace design.

Temperature calibrations should be preferably based on, or at least checked by, mass spectrometric monitoring [6] of the pressure of elements with a well-known melting point [45]. Ideally, calibration should be made in the temperature range of the experiments to be subsequently performed. The accuracy of such calibrations depends on the amount of the reference material placed in the cell and on the rate of cycling temperature around the melting point. The purity of the temperature reference sample should be checked regularly to avoid cryoscopic temperature decrease by crucible dissolution or contamination by reverse effusion of volatile species from deposits previously accumulated in the furnace assembly. This calibration procedure can make it possible to verify that the temperature is uniform throughout the cell, that the thermocouple or the black-body cavity is correctly located and that the reading devices perform adequately. Up to the melting point of gold, the melting points defining the International Temperature Scale, ITS-90 [45], provide the highest accuracy. In the 1400–2200 K range, a pyrometer has been developed [46] with an accuracy within 0.5 to 1 K of ITS-90, extrapolated with use of the Planck law.

4.2 Mechanical assembly of Knudsen cells

An important consideration in the design of a Knudsen cell is to make certain that the temperature is uniform throughout the inner cavity where evaporation takes place and the region where the temperature is measured. Gradients cause significant problems. These include incorrect temperature readings, condensation on cool parts of the cell, clogging at the orifice in extreme cases, and other perturbations. In the presence of purposely introduced gradients, it was shown [47] that the mass spectrometrically measured fluxes tend to be controlled by the temperature at the location of the sample. Knudsen cells should preferably consist of two more or less symmetric, heavy (compared with the sample), tight-fitting parts rather than of a large body and a loosely fitting lid. The two parts should mate with a joint that is either tapered, well ground and friction-fitted, screwed, or welded to avoid temperature gradients or gas leaks and to retard creeping of fluid samples through the cell joint. For chemical, technical, or economic reasons, use of cells completely made of the same material may be precluded. The Knudsen cell in the strict sense has then to be located in a surrounding shell or envelope. This outer shell should possess the thermal properties described above for cells made of a single material. In the temperature range where they can at present be used, heat pipes surrounding the cells [48–50] may facilitate thermal equilibration. Temperature uniformity in cells is also related to the nature and geometry of their associated furnace and shield assembly. The cells should be supported on legs as thin as is compatible with mechanical stability or be mounted in such a way as to avoid major heat loss through conduction into the support.

Resistance furnaces, heated with W, Mo, or Ta resistors and/or electron bombardment of the Knudsen cell or of its envelope may be used in the high-temperature regime. Resistance furnaces with a heater consisting of a single foil, mesh, or wound resistor as well as cells heated by electron bombardment have proven to work satisfactorily in many instances. Multiple shields are often designed into the heated system to minimize temperature gradients. Care should be taken to simultaneously minimize collision of effusing gases with the furnace or hot shields. These may indeed give rise to spurious contributions, either immediately by reflection, or over time, as material deposited in the shield region is reemitted, in particular when the temperature is raised.

4.3a Effusion orifices and equilibrium in cells

A properly collimated molecular beam is to be formed under circumstances such that there exists a known relation between the flux of each gaseous species in the system and its partial pressure in the cell. When using a Knudsen cell, the mean free path within the cell should, therefore, remain larger than

the diameter d of the effusion orifice. This condition is in practice met when the total pressure p is such that p/d does not exceed 1 Pa/mm.

The kinetic theory of gases shows that, for each gaseous species j, the differential effusion flow expressed in amount of species j per time (SI units mol s^{-1}) is given by the Hertz–Knudsen equation:

$$dn_j/dt = p_j aC/(2\pi M_j RT)^{1/2} \tag{3}$$

In this relation, p_j and M_j respectively represent the partial pressure and the molar mass of the species j and T the cell temperature, R the gas constant, a the area, and C the Clausing factor of the orifice [51]. The latter factor is the transmission probability of the actual orifice referred to that of the corresponding "ideal orifice" in an infinitely thin lid, for which $C = 1$.

Concordant values have been calculated [52–56] by different authors for the Clausing factor of truly cylindrical effusion orifices. In the range $0 \le l/r \le 5$, the usual one in effusion studies, this factor can be represented [53] within better than 0.1 % by the empirical relations 4–6. In these relations, $L = l/r$, l being the length and r the radius of the orifice.

$$C = C_1 - C_2 \tag{4}$$

with

$$C_1 = 1 + (L^2 + 4) - (L/4)(L^2 + 4)^{1/2} \tag{5}$$

$$C_3 = \frac{\left[\left(8 - L^2\right)\left(L^2 + 4\right)^{1/2} + L^3 - 16\right]^2}{72\left[L\left(L^2 + 4\right)^{1/2}\right] - 288\ln\left[L + \left(L^2 + 4\right)^{1/2}\right] + 288\ln 2} \tag{6}$$

Clausing factors have also been computed for conical orifices [54]. The latter data and a detailed discussion [57] for "spherical" orifices afford correction for imperfections introduced by machining.

An effusion orifice is rarely perfectly round. To determine its area, good practice includes careful optical microscopic observation. Calculating the actual area and using an effective radius is generally adequate if l/r is small. One should correct for thermal expansion of the orifice.

When the pressure increases in the Knudsen cell, the mean free path λ of the molecules in the gas phase can become comparable to the orifice diameter. At that stage, called "failure-of-isotropy", collisions between species in the vicinity of the effusion orifice start to modify the effusive flow process. The resulting corrections for eqs. 4–6 imply—in principle—that eq. 3 remains valid for K larger than 8, where $K = \lambda/2r$ is the Knudsen number. Calculated and measured correction factors agree to within better than ±2.5 % for Knudsen numbers ranging from 0.4 to 8. This leeway allows extension of pressure measurements with effusion cells by up to a factor of 20 beyond the limit (~10 Pa) usually ascribed to Knudsen effusion experiments. More extensive discussions of the effusion method, applications, and results are presented in [57,58].

It was assumed above that the pressure in the cell remains close to its equilibrium value, i.e., that

- the number of molecules removed from the system per unit time for sampling purposes is small compared to the number of molecules entering the gas phase as a result of processes taking place within the system and
- the rate of gas interaction with the sample is much greater than the effusion rate.

The vaporizing surface A of the sample should consequently be as large as possible compared to the effective effusion area, aC.

For some solids, the rate of surface reactions may cause the vaporization process to be slow, a regime often called retarded or hindered vaporization. The measured pressure then depends on the ratio $f = aC/A$ and on the conductance of the cell [59,60],

$$p_{eq} = p_m[1 + f(1/\alpha + 1/W_A - 2)] \quad (7)$$

where α is the evaporation coefficient [61] of the effusing species, W_A the Clausing factor of the inner cell body, p_m the measured pressure, and p_{eq} the equilibrium pressure. This relation was confirmed by Monte-Carlo calculations [62]. It is to be stressed that upon using eq. 7, one presumes that the vaporization coefficient remains constant and independent of the degree of vapor saturation over the pressure range between p_m and p_{eq} (see [61,63]).

Only if this assumption is valid may one extrapolate p_m against $f\,p_m$ by varying the orifice size and obtain p_{eq} from the intercept and α from the slope. Nonlinearity of such a plot [63], or an extrapolated equilibrium pressure clearly different from the value reliably determined with other methods [64], may indicate a complex vaporization mechanism in which vaporization and condensation coefficients depend upon the degree of saturation of the vapor. It may then be difficult to obtain an equilibrium vapor pressure from effusion measurements. To acquire information about vaporization or condensation coefficients under such circumstances, one must also be careful to define vaporization and condensation coefficients precisely [61]. In practice, instrumental limitations may prevent measurement at small enough orifice sizes that the assumptions underlying eq. 7 apply.

Use of porous or powdered samples to increase the sample surface area has been critically discussed [63]. An element or a compound added to a system as a vaporization catalyst [13] should be verified not to give rise to chemical transport. In the case of graphite, for example, enhanced volatility in the presence of platinum is largely due to formation of the very stable molecule PtC(g) [65].

How close the open Knudsen cell system actually is to thermodynamic equilibrium can be readily verified by checking whether or not absolute pressures, ratios of pressures, or reaction quotients depend on the area of the effusion orifice at constant composition and surface area of the sample.

In concluding this section, it is recommended that $f = aC/A$ ratios be reported for pressure measurements based on use of Knudsen cells in order to facilitate intercomparison of experiments and results reported by different authors.

4.3b Orifices and equilibrium in cells for high-pressure supersonic sampling

The sampling orifice—usually called the nozzle—in a high-pressure sampling system is generally much smaller than for a Knudsen cell and typically is less than about 0.1 mm in diameter. Its size and shape are subject to gas dynamic constraints [15,66,67]. Often, it is located at the apex of an inverted 45° degree cone pointing back toward the sample, although successful designs using a flat plate with an imbedded 45° conical orifice have been reported [15]. Important conditions imposed on supersonic nozzles are that they be designed to withstand the pressure differential and produce a nearly laminar flow.

Equilibration in the high-pressure cell depends strongly on the residence time of the carrier gas over the sample, as is discussed for the transpiration method [68]. If it is too short, the escaping gas is undersaturated and deduced pressures are too low. If the residence time is too long, the gas can become supersaturated, resulting in deduced pressures higher than equilibrium values. In between, a saturation plateau region is generally found for a range of flows. It is necessary to test for the presence of such a regime to avoid being confronted with a cell or a system for which equilibrium cannot be established. Common causes of such situations are excessive back-diffusion of sample material into the cooler upstream regions or an orifice improperly sized for the pressure regime. When the composition of the vapor is complex, polymeric species usually show the effect of undersaturation before the

monomer does. In some cases, this is related to evaporation and condensation coefficients discussed above.

4.4 Effusive molecular beam sampling

The molecular beam to be analyzed is, in principle, defined by the Knudsen cell orifice and the entrance of the ion source. The corresponding solid angle for detection of effusing species ranges from 10^{-4} to 10^{-3} steradian. To restrict transfer of energy and deposition of matter emitted by the cell, the latter is surrounded by radiation shields. The beam crosses openings in these shields and additional collimating orifices before entering the ionization chamber through an aperture that mostly is attached to (or part of) the ion source. Refrigerated perforated plates or traps may also be interposed between the cell and the ion source.

The various openings or connections between differentially pumped compartments generally delimit a larger solid angle than do the effusion orifice and the entrance aperture of the ion source. Extraneous gaseous species formed in or scattered from various locations within the furnace can hence reach the ion source [69–71]. Methods to detect adventitious contributions to the beam include measuring the intensity distribution or "beam profile" with a movable slit [4,69,70] or a blade [71] and determining a phase shift, where synchronous measurement of a modulated beam is performed [72,73].

Quantifying the effects of extraneous species can be problematic when surface diffusion of adsorbed species along the walls of the effusion orifice results in only a small difference between the observed and the calculated intensity distribution or that recorded for supposedly well-behaved reference substances. This problem was already discussed in a previous analysis of the actual behavior of effusion cells [57] and may be an important source of error when the orifice area is quite small. Sampling species in a cone comprised within the steric angle defined by the effusion orifice, i.e., viewing inside the effusion cell [50,74] circumvents collecting extraneous species.

4.5 Supersonic molecular beam sampling (SMBS)

For high-temperature systems with total pressures in the range 100 to $\geq 10^5$ Pa (1 bar), beams for mass spectrometric analysis are generated by supersonic sampling techniques. These can have special consequences with respect to ionization processes and cross-sections (see Section 6.5). The expanding jet from the supersonic sampling nozzle is skimmed by a second inverted cone (typically with a 30° included angle). The orifice diameter at the apex of this skimmer cone is chosen to just fill the entrance aperture of the ion source. Typically, the solid angle for formation of the molecular beam is located between 10^{-5} and 10^{-4} steradian. Unlike with effusive beams, molecular contributions from the outer surface of the cell generally cannot reach the ionization source. The skimmer itself also acts as a major pressure reduction element and removes gas outside the sampling solid angle from the nascent molecular beam.

In a properly pumped system, the Mach disk is too weak to be a major stagnation point. A skimmer orifice located ~120–150 nozzle orifice diameters downstream generally produces near-optimum beam intensities. The exact position depends on cell pressure and on details of the orifice geometry and is best found empirically. The optimized location should be verified not to change significantly over the range of source pressures and temperatures investigated, or provision made to reposition the skimmer during experiments.

The sampling and measurement process varies from continuous to pulsed. For most studies, pulsed methods are either preferred or essential: they include use of mechanical choppers to modulate continuous beams [15,75] and thermal pulsing of the vapor [76] or of the condensed [18] sample prior to molecular beam production.

In the transpiration method, total pressures of the sample and the carrier gas together, up to about 10^5 Pa, are readily accessible, depending on pumping capacity in the nozzle-skimmer region. Detection

limits are set by the cell design and by the requirements that reverse transport of the sample be minimal and that flow rates be sufficient to avoid supersaturation of the carrier gas [66,67]. A typical total pressure range is ~5 to ~100 kPa with detection limits for species down to 1 ppm.

4.6 Ion, electron, and molecular beam intersection

The molecular beam is crossed with a beam of electrons in the ion source of the mass spectrometer. Two configurations are used. In one, the electron beam, the molecular beam, and the ion beam are mutually perpendicular. In this type of assembly, the ionization chamber can be quite open. The molecular beam may then traverse the latter without hitting its walls. Other advantages of the perpendicular assembly are that the effusion orifice can

- serve as a black-body hole for temperature measurement by optical pyrometry;
- be visually inspected to assist in properly aligning the effusion cell and the molecular beam; and
- be observed in order to detect surface migration, creeping, or intergranular penetration, especially when these phenomena modify the emissivity of the cell area surrounding the effusion orifice [69,70].

Analysis of the intensity distribution in the molecular beam may often be corroborated.

In the alternate configuration, the extracted ion beam is coaxial with the molecular beam. It is then difficult to avoid interaction of species in the molecular beam with plates within the ion source, where the vapor species may scatter, condense and re-evaporate, or form new volatile by-products by surface recombination. Such processes are important potential sources of error in the co-axial assembly when volatile species are analyzed. Condensable species may also influence the performance of the ion source by modifying the effective work function of the electrodes and by forming insulating or conducting layers.

Formation of spurious ions in the source region [77] and observation of ions issuing in small amounts from the Knudsen or the transport cell [78] have also been reported. As the efficiency of ion sources is only ~10^{-3} to 10^{-5} in producing ions from neutrals, the relative importance of small incoming ion populations can occasionally be significant, especially at very high temperatures, such as with laser-heated samples. Ion source contamination by alkali and other metals or compounds with low ionization energy E_i can also result in notable extraneous signals. The value of phase-sensitive detection in identifying extraneous signals and the presence of secondary reactions in the ion source has been demonstrated [79]. Simply turning off the source filament often also evidences the presence of spurious ions. Quantifying the importance of incident ions relative to that of neutral species is more difficult.

In all configurations, parallax can cause the signal to depend on the entrance angle of the molecular beam and thus on displacement of the cell. Restrictive collimation, in which the molecular beam to be analyzed is defined by apertures interposed between—and smaller than—the orifices of the Knudsen cell and the ionization chamber, eliminates parallax errors [74].

4.7 Residual pressure and measurements for "permanent" gases

Conventional vacuum gauges, properly installed to monitor the source region and other sections of the MS as well as use of the instrument as its own vacuum analyzer and leak detector, usually provide adequate monitoring of the residual (or "background") pressure that arises from the ubiquitous presence of so-called permanent, or noncondensing, gases (including atmospheric gases, water vapor, volatile hydrocarbons from inadvertent fingerprints, pump oil, and the like). The following considerations nevertheless seem warranted.

- The residual pressure in the ion source and the steady-state number density in the molecular beam should be low enough to avoid second-order processes such as molecule–ion interactions. In the

present context, this type of process would correspond to reaction between ions formed in the ionization chamber and neutral species present in the latter as constituents of the molecular beam or of the residual gas. To prevent occurrence of such phenomena, the pressure in the ion source should be definitely lower than 1 mPa, and the local steady-state number density in the molecular beam should be correspondingly low. Achieving the required vacuum requires attention to pumping capacity when gases such as H_2, N_2, O_2, H_2O, CH_4, CO, CO_2, etc. are either formed by decomposition of the system studied or intentionally introduced into the effusion cell. In the case of condensable species, and when the distance between the effusion orifice and the ion source is about 5 to 7 cm, the more stringent upper pressure limit for effusion to occur under Knudsen conditions simultaneously ensures that the maximum allowable steady-state number density is not exceeded in the molecular beam during traversal of the ion source.

- In SMBS, differential pumping and separation of the sampling orifice (nozzle) and ion source regions are required, together with attention to the design of the sampling orifice and of the downstream "skimmer" or secondary beam-defining orifice. The large number of molecules leaving the sampling orifice may indeed cause significant fluid dynamic effects, such as strong shocks and stagnation zones. The possibility that gas scattered from such regions enters the ion source at angles other than the collimation solid angle requires that the direct molecular beam be modulated, typically with a chopper or by modulation of the vapor-producing process, as in laser vaporization. To separate signals from background interference, the ion signal is then detected and processed with a phase-sensitive detector, typically a lock-in amplifier, or other time-resolved detector amplifiers (such as signal averagers, multichannel scalers, boxcar amplifiers, etc. operating synchronously with signal production). The absence of background contributions should, nevertheless, be ascertained. Attention to design of the vacuum chambers and use of high-speed pumping are both required to minimize gas dynamic effects. In a properly constructed high-pressure sampling system, the molecular beam density in the ion source is no higher than in investigations based on Knudsen effusion because longer path lengths are typically used in the former. Differential high-speed pumping ensures residual pressures below ~0.1 mPa in the ion source and precludes undesirable ion–molecule collisions.
- In both low- and high-pressure sampling, scattering of molecules from the molecular beam by residual gas must obviously be avoided. The residual pressure in successive differentially pumped compartments should be low enough for the mean free path to be much larger than the length of each compartment, which typically requires pressures $\leq 10^{-2}$ Pa in the nozzle skimmer-chamber and ≤0.1 mPa in regions where molecular beams are formed or present.
- In KMS, reverse effusion may occur when the thermochemical conditions in the cell imply local reduction of the partial pressures of some constituents of the residual gas. In the latter, oxidants such as O_2, H_2O, and CO_2 are often more abundant than reducing constituents such as CH_4 and other hydrocarbons. Influx of residual gases with partial pressures in the μPa region or lower may hence either prevent complete deoxidation of the sample studied, cause slight oxidation, or lead to steady-state conversion of entering O_2, H_2O, etc. into effusing metallic oxides [80,81]. In high-pressure systems, gas dynamic flow generally precludes such effects.
- The residual gas pressure along the trajectory of the ion beam in the analyzer must be low enough to avoid scattering and collision-induced decomposition of molecular ions. The acceptable residual pressure, hence, depends somewhat on the particular dimension of each mass spectrometer. The residual pressure should also be low in the detector housing to avoid altering the yield of the secondary electron multiplier. In magnetic single or double focusing instruments, the beam-defining slit often acts as a differential pumping orifice and makes it possible to maintain UHV conditions in the analyzer and/or detector housings. Especially where air-sensitive multipliers are used, valving off the detector (and the source) region is desirable whenever the MS is opened.
- When the ion source and cell regions are enclosed in separately pumped housings, the location, nature, and shape of the molecular beam shutter are important parameters for the proper meas-

urement of those effusing gases that are also present in the residual gas or that cannot be distinguished therefrom within the resolving power of the MS. A shutter more or less tightly closing the aperture between the furnace and ion source regions could indeed generate adventitious contributions to the genuine effusing beam when the residual partial pressure of some interfering gas is higher in the furnace housing than in the ion source region [74]. Any shutter should actually be mounted in such fashion that its operation does not appreciably influence the pumping speeds in and between compartments. Sufficiently large pumping capacities minimize such problems.

4.8 Mass bias

Mass bias (discrimination) designates contingent systematic differences, dependent upon atomic or molecular mass rather than on chemical nature, between quantities to be measured and those actually observed. Such quantities here include partial pressures and ion intensities or their ratios.

In the molecular beam-forming process, Knudsen effusion has been shown to produce a $\cos\theta$ intensity distribution about the normal to the orifice, essentially independent of mass. The Hertz–Knudsen relation, eq. 3, takes account of the dependence of the rate of effusion on mass.

High-pressure sampling generally results in strong forward-peaking of the nascent beam, often according to $\cos^n\theta$, $n \geq 4$ being dependent on cell pressure, orifice diameter, and mass. The tendency is for heavier species to be concentrated toward the beam centerline, a phenomenon known as Mach focusing. This effect can, to some extent, be compensated for by choosing a carrier gas with a mass comparable to the average molecular weight of the species in the beam. In practice, it is necessary to calibrate for the effect, typically by adding to the carrier gas, at the percent level, a known mixture of inert gases up to Xe or perfluoro compounds, for instance, at higher masses. This procedure actually provides measurement of the overall bias of the complete system during high-pressure sampling and mass analysis.

Charged particles formed in the ion source are drawn out and accelerated into the analyzer to measure the mass-to-charge ratio and the intensity for each ion present. The MS generally comprises an ion source, a mass analyzer, a detector (Faraday cup and/or multiplier), a detector amplifier (electrometer or ion-counting equipment), and a data recording system [82]. Mass bias can, in principle, occur at each of these stages. The recorded information may, hence, be vitiated by convolution of a mass dependence of the draw-out efficiency from the ion source, a mass-dependent transmission coefficient through the mass-analyzer, and a mass-dependent response of the detector for the ions observed.

Stray or auxiliary magnetic fields in the ion source influence the trajectories of charged species as a function of their masses and energy. They may cause observation of peculiar ionization efficiency curves (see below) and induce mass bias in the extraction yield from the ion source. When possible, it is, therefore, preferable to use ion sources without magnetic electron beam confinement and with good magnetic shielding. There are, at present, no indications for a temperature dependence of the extraction yield of ions formed from species in the molecular beam. However, it is necessary that the ion source be protected against thermal radiation from the oven assembly.

Pronounced bias is generally ascribed to quadrupole mass spectrometers, for which adjustment of potentials on various elements such as the source, extraction, and focusing lenses can modify transmission over the mass range. Frequent calibration against a standard gas mixture, or some other known mass spectrum, is therefore desirable. Quadrupoles can be tuned for transmission to be either proportional to $1/M_k$ or relatively constant within a certain mass range. Bias often assigned to the quadrupole analyzer itself actually results from use of a low draw-out potential for ions from the source into the analyzer, typically 5–30 V, compared to 2–8 kV in magnetic instruments. This low energy causes significant differences in dwell time for ions in the analyzer, with consequent differences in selectivity. Making the draw-out potential proportional to mass can reduce analyzer bias significantly. In the absence of sufficient post-acceleration between the quadrupole analyzer and the secondary electron multiplier, the ions impinge with relatively low energies onto the first dynode of the detector. This dynode,

however, increasingly discriminates against charged species of higher mass when their momentum is lower than the threshold value required for effective conversion of ions into secondary electrons. In recent years, this problem has been overcome through use of a separate "conversion" dynode, operated at 5–10 kV or more [82]. The latter bias effect can also be significant for other analyzer-detector arrangements and particularly for very high-mass ions.

The efficiency of electron multipliers may be a function of the mass and of the chemical nature of the ion [83]. For secondary electron multipliers used with electrometers in the analog detection mode at constant post-acceleration, the mass dependent factor has been summarized for atoms [84,85]. Measured yields have been compared with a previously proposed—and commonly applied—relation, $\gamma_k \propto q\, M_k^{-1/2}$, where γ_k is the multiplier yield, q the charge on the ionic species k, and M_k its mass [83]. An alternate dependence, $\gamma_k \propto q\, M_k^{-0.4}$, has been proposed for $M_k \geq 19$ u [85]. Yields measured for atomic ions may deviate by up to ±30 % from this relation and appear to depend on their electronic structure [83–86]. For molecular ions [87], the yield depends on the degree of decomposition and partition of kinetic energy at the first dynode (or another surface). Their yields may, therefore, be somewhat higher than for atomic ions of the same mass [88,89], but no general rule seems to have been proposed for electron multipliers as was done for photoplates [90].

Linearity of electrometers or counting equipment and of associated recorders is rarely an issue for state-of-the art equipment, but still should be checked. In particular, both for pulse counting and analog detection, the multiplier response is known to depend on the flux, whereas pulse-counting recorders are often strongly limited in their ability to separate pulses at high count rates.

The evolution of technology in electronics and secondary electron multipliers explains the current preference for ion pulse counting [89,91,92], but there is no satisfactory solution to accomplish vector phase-sensitive detection. Fixing an appropriate counter discrimination threshold requires analyzing the performance of the system. This remains necessary even when the beam to be detected is momentarily intercepted ("shuttered"), and the net ion signal taken to be the difference between counts recorded in the presence and absence of an incident molecular ray. The main requirement is that background pulses originating from the electronic chain, and low-level noise in the electron multiplier, be clearly separated from genuine events. The resulting discriminator threshold may be but a compromise between loss of counts and undue noise. In the case of partial amplitude overlap between background and incoming pulses, a mathematical treatment can be used to evaluate the mass bias associated with the chosen threshold on the basis of experimental data. For a correctly thresholded ion pulse counting system, the uncertainty is proportional to $1/\sqrt{n}$, where n is the true number of incident ions.

The speed of the detection chain and especially the multiplier pulse transit behavior govern the limit for linearity at a high counting rate. "Pulse pile-up" occurs for high counting rates, usually more than 2×10^7 counts/s for the most rapid systems. A simple formula corrects for overlap of incident ions [89]:

$$n = n_o/(1 - n_o\tau) \tag{8}$$

where n and n_o are the true and observed counting rates and τ is the resolving time of the complete detection chain. In practice, dead-times are such that the above correction is small until pile-up causes pulses to overlap to the extent that they cannot be distinguished.

Both analog and counting systems should be calibrated in the upper range of signals against a properly operated Faraday cup. The main advantage of pulse counting is that use of high voltages in the so-called "saturation region" can make the conversion efficiency essentially constant and independent of the nature of the incident ion—hence, rendering mass bias in the multiplier quite small over broad mass ranges.

5. CHEMICAL FACTORS

Ideally, the substance investigated should be pure and the container inert. In practice, impurities may be present in the sample studied while more or less pronounced alloying, reduction, or oxidation may take place by interaction with the container. Such chemical interactions are avoided in laser vaporization mass spectrometry (LVMS) [93], where the sample serves as its own container, local equilibrium nevertheless being attained by inertial confinement of the Knudsen layer.

5.1 Mass spectrometric observations

Instead of by inference, as in many other methods, mass spectrometric analysis of the vapor can readily identify the presence of unwanted or unexpected chemical factors via the observation of:

- volatile impurities unrelated to the system;
- evolution in composition by unexpected vaporization processes during conventional outgassing;
- gaseous species formed by interaction with the container;
- lack of reproducibility in absolute or relative intensities when cycling temperature, owing to ongoing interaction between the sample and the container;
- in systems with more than one component, minute to large modifications in intensity ratios for different gaseous species upon placing aliquots of the same sample in cells made of different materials;
- time-dependent behavior in systems expected to be univariant;
- hysteresis effects in nonstoichiometric compounds with a congruently effusing composition that varies with temperature [94]; and
- distortion of the intensity distribution in the molecular beam when wall penetration, surface migration, or creeping of liquids leads to vaporization from an area larger than the effusion orifice.

Full mass spectra should, therefore, be recorded at a sufficient number of temperatures and at different times during an experiment. During the measurements and the subsequent interpretation of the spectra, the possibility of fortuitous interference of different atoms or molecules with the same m/q (mass/charge) ratio should be considered if the mass resolution of the instrument is insufficient for their separation. Outgassing of the cell or crucible in situ as a preliminary step, and recording spectra in the contemplated temperature interval in order to identify volatile impurities is recommended. In SMBS, the same applies to analysis at the ppm level of the carrier gas as delivered to the system. Micrographic, X-ray, chemical, microprobe, or other analyses of the sample, of the cell or crucible, and of the lid after the experiment also provide useful information. Detailed information concerning the origin, preparation, and history of samples is highly desirable.

5.2 Thermodynamic equilibrium in cells

Formation of alloys or, more generally, of solid solutions by reaction of the sample with the cell material can often be avoided or minimized by selecting the latter on the basis of existing phase diagrams. Thermodynamic cross-checks can be performed, taking into account all measured ion intensities to identify:

- partial lack of equilibration;
- significant crucible interaction;
- incorrect sensitivity estimates; and
- incorrect calibration of the mass spectrometer for some gaseous species.

In activity determinations, the Gibbs–Duhem relation should be integrated whenever possible to check the consistency of simultaneously measured activities. The experimenter should bear in mind that

mass spectrometric determinations lead, in many cases, to more information than is needed to define a chemical system because the gaseous phase often contains several thermodynamically nonindependent atoms and molecules. This additional information can be used to cross-check the measurements and to improve the interpretation (but not the precision) of the mass spectrometric and of the thermodynamic data.

5.3 Physicochemical behavior of cells

Other causes of inaccuracy best mentioned here are possible deviations from the cosine law on which the relation between rates of effusion and partial pressure is based. This problem is inherent to the Knudsen effusion technique, whether combined or not with mass spectrometric analysis of the vapor. The use of calculated transmission probabilities or Clausing factors for the effusion orifices supposes genuine effusion and absence of specular reflection or surface diffusion along the orifice walls [57]. Such parallel flow increases the deduced vapor pressures in the proportion of the diffusional to the total flow. The mass spectrometer assists in uncovering deviations from the cosine law and their dependence on the nature of the effusing molecule. Such effects have in reverse been used in the analysis of complex vapors [95].

The influence of surface migration and specular reflection of molecules on the orifice walls has been summarized [96]. A correction formula that depends on shape and size of the orifice and on the mean free path for surface diffusion has been proposed. Some recommendations to detect and minimize extraneous flow relative to genuine effusion are:

- compare experimental runs using different lid materials;
- use large orifices rather than small ones to minimize the surface contribution relative to genuine effusion;
- use large cells with properly chosen orifice sizes and appropriate amounts of sample to ensure equilibration and, if of interest, to reduce the rate of change in composition of condensed phases;
- use cylindrical orifices in reasonably thick covers rather than apertures in very thin surfaces—so doing increases thermal inertia, reduces orifice cooling, and favors equilibration within the cell; and
- sample the effusing beam in a narrow solid angle to minimize or avoid [74] collecting species reflected from shields or furnace walls.

Diffusion or permeation of one or more constituents of the sample through the wall of the effusion cell [97] may likewise perturb measurements. The incidence of such processes has been limited in a number of instances by use of entire cells or of inserts made from high-density material, even from single crystals.

6. PHYSICAL FACTORS

In order to determine the chemical formula of the neutral species and the nature of the chemical reactions taking place in the sample cell, a variety of measurements is needed to characterize the neutral progenitor of each ion observed. The information so to be gained is also of importance in the later conversion of ion intensities into partial pressures.

A reasonable understanding of the ionization processes taking place in the atoms and molecules of the system studied and of the factors determining the relative importance of different ionization channels should be achieved. These processes obviously are fundamentally the same for rare gas and metallic atoms formed at high temperatures or for organic and inorganic molecules. Valuable information on the subject is available in classical and in recent monographs on collision processes in atoms and molecules [98–103] and on mass spectrometry [89,104–111], even when investigations at high temperatures are not highlighted. Attention is also drawn to very general threshold laws [112–115] describing

the idealized variation of cross-sections for excitation as well as for ionization near the minimal energy required for these processes to occur.

6.1 Ionization processes

The intensity for each ion is normally measured as a function of the energy E of the ionizing electrons to establish the ionization efficiency curve $I(E)$ and, in particular, to determine the appearance energy E_a, i.e., the minimum energy at which each ion is formed. For such measurements, the energy scale should be calibrated and its linearity verified under molecular beam conditions. The latter may preclude—or render quite approximate—calibration with permanent gases in a non-beam form. Calibration is, therefore, preferably performed at the beginning of the experiment with a small amount of a known, chemically inert substance that is more volatile than the system being studied. This added substance may be and commonly is the one also used to determine the sensitivity of the instrument, as described in Section 7.1. Later in the experiment, atoms found to be present in the gas of the system studied can also be used to calibrate the energy scale.

The minimum energy required to form a given ion is next compared with values [30,39,40] of the ionization energy E_i known from optical spectroscopy, photo-electron spectroscopy, other mass spectrometric experiments, quantum-chemical calculations, or empirical estimates. The distinction is thus to be made between an ion formed by direct ionization [4,9] of a neutral molecule, i.e., a parent ion,

$$A + e^- \rightarrow A^+ + 2e^- \qquad E_i(A) \tag{9}$$

$$AB + e^- \rightarrow AB^+ + 2e^- \qquad E_i(AB) \tag{10}$$

and an ion formed from a molecule with a higher molecular weight, i.e., a fragment ion

$$AB + e^- \rightarrow A^+ + B + 2e^- \quad E_a(A^+/AB) \geq E_i(A) + D(A - B)/e \tag{11}$$

$E_i(A)$ is the ionization energy of moiety A, $D(A - B)$ is the dissociation energy of the bond ruptured during the ionization process. The inequality sign takes into account that fragments can be produced on a repulsive potential energy curve and possess relative kinetic energy in excess of thermal values and that either or both of the moieties A and B can be formed in electronically or vibrationally excited states.

The intensity of each ion is normally measured as a function of temperature at constant energy of the ionizing electrons. In general, the two or more ions for which the intensity ratio is observed to change are not formed from the same precursor. This criterion is not unambiguous. The relative importance of parallel ionization channels in the same molecule can indeed vary with temperature [5,18,20,116–123].

The measurement of a threshold energy indicating direct ionization for a given system does not ensure that interfering dissociative ionization of other molecules remains negligible at higher energies of the ionizing electrons or when either the composition or the temperature of the system are modified.

The nominal value of E_i in each set of data points may differ from its true value for a number of reasons, resulting in random and/or systematic uncertainties. The reasons may include poor regulation of the ion source electron current, thermal expansion and/or mechanical instability of the source assembly due to heating by the electron-emitting filament (and temperature-stabilizing heaters in some sources), and degradation of insulators by stray deposits from the molecular beam or from residual gases, such as may originate from pump oils. The effective work function of the ion source assembly always causes an offset of the observed E_i from the true value. This offset is calibrated for with well known values of E_i.

Additional systematic uncertainty may be introduced when the contribution of some molecule to the total intensity I_i is deduced from measurements made in another laboratory, in another experiment in the same laboratory, or even in the same experiment under different circumstances of temperature or composition. The latter could, e.g., occur when dissociative ionization of AB to $A^+ + B + e^-$ and direct ionization of A to $A^+ + e^-$ replace one another as predominant processes depending upon conditions.

The low energy range of the ionization efficiency curve near threshold is the part generally exploited in studies of the type discussed here. In a number of instances, ion intensities for different species have, hence, been measured at different energies, so chosen that $(E - E_i)$ is constant or that E is just as high as is justified by the restriction $E_i\,(A^+/A) \le E \le E_a(A^+/AB)$. The investigator should preferably also examine the evolution in shape of the $I(E)$ curve up to 80–100 eV as a function of system temperature or chemical composition. Doing so often clearly shows whether two or more molecules lead to formation of a common ion. In conventional single-cell measurements, interference between parent and fragment ions is usually easier to detect if the difference $E_a\,(A^+/AB) - E_i\,(A^+/A)$ is large. The use of twin or multiple cells to compare $I(E)$ curves for different compositions of the gas phase circumvents conceivable undetected variation of ion source behavior between successive experiments [124].

When neutral beam velocity information is available, such as with transpiration mass spectrometry (TMS) [19], LVMS [93], or modulated-beam KMS [125], interpretation of fragment and parent ion intensity data is more straightforward, although the experiments are more complex.

Occasionally [126], formation of so-called metastable ions [104–111,116–118] is observed in mass spectrometers with a magnetic sector. These correspond to unimolecular decomposition of ions during transit between the ion source and the magnetic field. This process gives rise to the presence of broad peaks at nonintegral masses in the spectrum. To be observed, the lifetime of the decomposing ion is to be comprised within a rather narrow time interval [116–118]. The decomposing and the fragment ion are then simultaneously present in the spectrum. The importance of observing metastable transitions is that:

- such processes provide unambiguous identification of the precursor ion of the particular fragment ion;
- the precursor ion is usually but not necessarily the parent ion;
- measurement of the minimum energy at which the process is observed provides a better approximation to the appearance potential of the fragment ion (absence of kinetic shift); and
- a fraction of the decomposing ions is lost and appears neither as parent nor as fragment ion.

When ambiguities arise in the interpretation of $I(E)$ curves, modifying the chemical composition of the system and applying the mass action law is indicated to establish the proper relation between the actual neutral precursor and ion intensities measured at different values of m/q and E.

It may be noted in the present context that identical molecular ions are often encountered in spectra of solid samples obtained in spark source mass spectrometry (SSMS) [127] and in spectra produced by electron impact in vaporization experiments of the type discussed here. The two modes of forming ions are, however, quite different. In HTMS, ions are produced in single collisions of neutral species present in molecular beams with electrons of defined and generally low energy. In SSMS, ionization is mostly achieved [128] in RF sparks generated between two electrodes of the same material by a pulsed high AC voltage (25–100 kV). The species produced first in time include singly and multiply charged atomic ions [129]. The formation of molecular ions occurs later and is ascribed to plasma-chemical processes [90,129]. These presumably comprise ejection of neutral species and of ions from either electrode by sputtering and ion–molecule reactions, charge-exchange, ionization by collision with electrons or with neutrals in highly excited metastable states in the space between the electrodes. Intermetallic ions are, therefore, observed in SSMS not only when studying alloys, but also when the opposed electrodes are made of different pure metals [90]. Hetero-atomic molecular ions are likewise generated between electrodes prepared from mixtures of powdered graphite with nonconducting substances such as sulfur or oxides [129]. Observation of a given molecular ion in either one—or in both—of HTMS and

SSMS spectra hence establishes stability of this ion against unimolecular decomposition in the time elapsed between its production and detection. Such physical stability [130] does, however, not imply that the relative intensities for particular ions should be comparable in HTMS and SSMS spectra, nor that thermodynamic data for the neutral molecule corresponding to a given molecular ion can be deduced from SSMS observations, as can be done in HTMS by the procedures discussed below.

Selective post-ionization by electron impact of neutrals formed by sputtering of Cu and Ag actually showed [131] that, relative to the atom, the abundance of di- and poly-atomic molecules (clusters) so formed is much higher than it is in thermally produced vapors. Determination of $\sigma(Ag^+_2/Ag_2)/\sigma(Ag^+/Ag)$ was thereby greatly facilitated [132].

6.2 Ionization cross-sections of atoms

Among several sets [133] of calculated ionization cross-sections, four in particular [134–139] are or have been commonly employed in mass spectrometric studies at high temperatures.

The first set was introduced by Otvos and Stevenson [134], who drew attention to a theoretical result of Bethe that the ionization cross-section of an atomic electron with quantum numbers (n, l) is approximately proportional to the mean square radius of the electron shell (n, l). Accordingly, using hydrogen-like wave functions for valence electrons, these authors calculated atomic ionization cross-sections for the elements with Z = 1–56, 80, 81, and 82.

Gryzinski [135] and Lin and Stafford [136] used the classical theory of inelastic collisions—the binary encounter approximation—for each orbital l to obtain:

$$\sigma_l(E) = (\sigma_o/E^2_{i,l})g_l(x) \tag{12}$$

with

$$g_l(x) = \frac{1}{x}\left(\frac{x-1}{x+1}\right)\left[1+\frac{2}{3}\left(1-\frac{1}{2x}\right)\ln\left(2.7+(x-1)^{1/2}\right)\right] \tag{13}$$

$x = E/E_{i,l}$, E is the incident electron energy, $E_{i,l}$ the binding (or ionization) energy of the electron in orbital l, and σ_0 a constant, the value of which for an elementary charge is 6.56×10^{-14} eV^2 cm^2.

Lotz [137] proposed an empirical formula, within the Bethe formalism, with σ_l summation for the various accessible orbitals:

$$\sigma = \sum_l a_l q_l \frac{\ln(E/E_{i,l})}{EE_{i,l}}\left\{1-b_l\exp[-c_l(E/E_{i,l})]\right\}, \text{ for } E \geq E_{i,l} \tag{14}$$

The coefficients a_l, b_l, and c_l are calculated using experimental ionization cross-sections and interpolation along rows and columns of the periodic table.

Mann [138,139], with equations similar to those of Bethe, the Born approximation and some additional assumptions associated with its use at low energy, calculated the contribution σ_l of the electron l (if not s^1) to the total ionization cross-section σ as:

$$\sigma_l = AN_l\frac{<r^2>_l}{E^{3/4}}\ln\left(\frac{E}{E_{i,l}}\right)^{3/4} \tag{15}$$

A is the Bethe coefficient [134,138], N_l is the number of electrons in shell l with orbital radius r. For s orbitals with a single electron, the formula becomes:

$$\sigma_l = AN_l\frac{<r^2>_l}{E}\ln\left(\frac{E}{E_{i,l}}\right) \tag{16}$$

Relative cross-sections so obtained were normalized to the value 2.83×10^{-16} cm^2 for Ar at the maximum of the cross-section [138]. The presently accepted value is 2.62×10^{-16} cm^2 (see Table 2).

Orbital radii virtually identical with those calculated by Mann [139] have been computed by Desclaux [140] for the elements with $Z = 1$ to 120.

Bell et al. [141], and Lennon et al. [142], in the course of assessing experimental cross-sections, proposed:

$$\sigma_j(E) = \frac{1}{E E_{\mathrm{i},j}}\left[A_j \ln\left(\frac{E}{E_{\mathrm{i},j}}\right) + \sum_{k=1}^{5} B_{jk}\left(1 - \frac{E_{\mathrm{i},j}}{E}\right)^k\right] \quad (17)$$

The Bethe factor A_j and the coefficients B_{jk} are fixed for each species j, by taking into account measurements at low energy (≤100 eV), utilizing the Born approximation at high energy (≥300 eV), and scaling for atoms and multicharged ions with the same number of electrons. Least-squares adjustment may also be used. This tabulation is presently limited to singly and multiply charged ion production for elements from H to Ni.

In the framework of the present project, Mann's total cross-sections [139], calculated by summing the contributions of all accessible shells and subshells, have been fitted [143] according to relation 17. Coefficients are presented in Table 1 for practical use. Figure 1 shows a typical $\sigma(E)$ curve, calculated using data from Table 1, together with the original curve calculated by Mann [139].

The experimental determination of ionization cross-sections for permanent diatomic gases and relatively volatile metallic vapors was critically discussed by Kieffer and Dunn [144]. These authors considered the incidence of uncertainties in extraction, transmission, and detection coefficients, summarized data reported up to 1966 (high-temperature molecules excluded) and discussed the importance of autoionization for a number of elements.

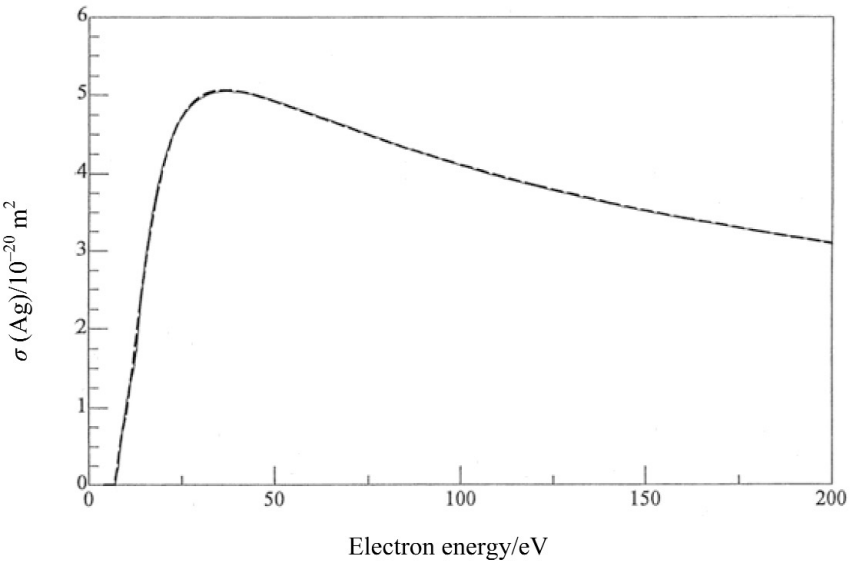

Fig. 1 Energy dependence of the cross-section for the process $Ag + e^- \rightarrow Ag^+ + 2e^-$ as calculated by Mann [139] (thin line) and by Program Sigma [143] (heavy line) with fitting coefficients reproducing the tabulated data (see Section 6.2).

Table 1 Coefficients for calculating ionization cross-sections of atoms from tabulated data [139] with the eq. $\sigma_j(E) = \frac{1}{E\,E_{i,j}}\left[A_j \ln\left(\frac{E}{E_{\mathrm{i},j}}\right) + \sum_{k=1}^{5} B_{jk}\left(1 - \frac{E_{\mathrm{i},j}}{E}\right)^k\right]$ (see Section 6.2 and ref. [143]). $E_{\mathrm{i},j}$ is the first ionization energy of element j, E is the energy of the incident electron. The equation, with the coefficients in the table, gives $10^{20}\ \sigma_j(E)/\mathrm{m}^2$.

Element	Z	E_i/eV	$10^{20}\ A_j$/m^2 (eV)^2	$10^{20}\ B_{j1}$/m^2 (eV)^2	$10^{20}\ B_{j2}$/m^2 (eV)^2	$10^{20}\ B_{j3}$/m^2 (eV)^2	$10^{20}\ B_{j4}$/m^2 (eV)^2	$10^{20}\ B_{j5}$/m^2 (eV)^2
H	1	13.5980	110.838 256	3.840 825 75E-4	–8.097 393 7E-4	7.563 482 78E-3	–0.013 509 357 46	7.941 023 97E-3
He	2	25.8820	1066.964 35	–790.195 11	–242.653 77	–584.733 13	728.020 91	–763.370 00
Li	3	5.391 00	337.080 47	–95.269 63	197.652 34	–1001.870 75	1589.414 90	–955.545 96
Be	4	9.322 00	2538.844 56	–2064.660 52	298.951 61	–5467.114 89	8361.965 32	–5822.521 91
B	5	8.298 00	1997.269 43	–1711.644 56	–2096.856 80	2463.383 90	–336.148 29	–2234.354 17
C	6	11.2590	2437.805 40	–2008.795 33	–2365.629 78	4009.877 66	–3549.506 15	–466.669 59
N	7	14.5320	2808.827 82	–2260.730 69	–2404.968 54	4930.943 22	–6029.708 03	1120.751 25
O	8	13.617 00	2514.260 15	–2514.831 07	1276.043 47	–8358.117 63	12 492.050 10	–7670.342 96
F	9	17.422 00	3098.676 40	–2725.523 92	1383.145 34	–11 477.614 24	17 378.573 21	–10 286.523 21
Ne	10	21.564 00	3409.692 77	–2916.241 63	1369.733 92	–11 090.489 79	15 959.089 01	–9132.078 29
Na	11	5.139 00	671.101 16	–363.048 82	–341.345 16	64.043 83	341.316 43	–860.803 59
Mg	12	7.646 00	3351.158 22	–2842.461 77	642.618 94	–8800.535 39	13 852.035 95	–9640.550 11
Al	13	5.986 00	2757.727 48	–2554.592 38	152.581 36	–8869.836 20	16 940.227 33	–11 536.806 22
Si	14	8.151 00	3854.865 03	–3305.849 96	–1435.644 24	–4446.670 04	10 936.229 45	–9372.496 81
P	15	10.486 00	4819.476 14	–3995.057 13	–2539.611 57	–424.392 01	4408.452 44	–6383.005 55
S	16	10.359 00	4531.974 56	–4692.716 96	4664.469 15	–22 406.047 25	31 171.257 81	–17 545.760 16
Cl	17	13.017 00	5843.379 47	–5043.706 23	952.912 74	–16 227.622 56	26 862.262 17	–17 724.783 73
Ar	18	15.759 00	6941.283 81	–5926.300 95	779.307 05	–17 197.086 24	28 407.126 42	–19 126.945 01
K	19	4.340 00	1354.878 81	–850.176 52	–2020.882 27	4926.549 47	–6894.467 40	21 23.217 36
Ca	20	6.113 00	5097.215 00	–4409.255 36	–426.769 42	–8446.893 50	13 406.982 84	–11 140.024 80
Sc	21	6.540 00	4933.298 09	–4287.916 38	–353.262 96	–7537.502 61	11 917.791 67	–10 089.148 26
Ti	22	6.820 00	4963.242 53	–4308.447 06	–897.404 14	–6815.158 98	12 499.198 41	–11 024.694 81
V	23	7.062 00	4999.015 25	–4408.706 67	–258.769 67	–10 488.198 97	18 948.545 25	–14 620.225 58
Cr	24	6.765 00	2461.845 14	–2394.036 52	1341.116 90	–6666.566 95	9501.887 59	–6910.085 09
Mn	25	7.434 00	4651.476 71	–4234.058 96	1638.971 53	–17 782.813 12	29 665.260 48	–19 343.541 33
Fe	26	7.897 00	4197.737 95	–3761.109 61	1142.141 39	–13 066.140 77	21 413.927 63	–14 049.608 02
Co	27	8.279 00	4205.513 02	–3536.802 14	–1671.803 99	–3124.050 02	8345.708 00	–8110.290 14
Ni	28	8.675 00	4325.626 52	–3656.756 81	–1507.838 55	–4754.596 48	11 250.212 86	–9744.689 21
Cu	29	7.726 00	1770.717 44	–1487.163 72	–1739.784 69	4909.03693	–5765.760 68	1259.947 65
Zn	30	9.393 00	4557.402 88	–4014.615 57	231.161 37	–12 926.771 20	23 469.897 26	–15 914.381 64

Table 1 (*Continued*).

Element	Z	E_i/eV	$10^{20}\,A_j$/m^2 (eV)^2	$10^{20}\,B_{j1}$/m^2 (eV)^2	$10^{20}\,B_{j2}$/m^2 (eV)^2	$10^{20}\,B_{j3}$/m^2 (eV)^2	$10^{20}\,B_{j4}$/m^2 (eV)^2	$10^{20}\,B_{j5}$/m^2 (eV)^2
Ga	31	5.998 00	3081.558 31	–2969.707 85	798.574 22	–10 808.655 78	17 028.531 17	–10 672.837 30
Ge	32	7.885 00	4491.864 03	–3881.991 21	–2085.984 31	–3449.347 80	8111.578 82	–7848.215 41
As	33	9.815 00	6010.858 36	–5420.453 17	165.638 58	–13 701.475 83	22 253.776 19	–15 599.117 98
Se	34	9.752 00	5200.760 37	–5331.933 71	4926.203 21	–24 913.773 30	35 885.865 15	–20 882.582 75
Br	35	11.846 00	6614.869 04	–6030.969 84	3590.214 01	–25 823.515 18	39 356.321 51	–23 914.202 49
Kr	36	13.999 00	7994.878 97	–7231.878 12	3885.666 32	–28 541.981 62	43 204.671 13	–26 567.276 09
Rb	37	4.177 00	1580.642 02	–882.015 39	–3849.686 37	11 046.267 72	–16 011.732 02	6700.095 61
Sr	38	5.694 00	5675.724 91	–4854.462 19	–1596.148 51	–4927.918 78	7536.655 32	–8271.053 60
Y	39	6.482 00	6464.923 78	–5433.126 92	–2019.667 84	–5236.115 37	8607.747 39	–9561.750 42
Zr	40	6.837 00	6262.784 63	–5570.859 17	–1375.771 91	–4330.146 91	6436.953 45	–8064.864 96
Nb	41	6.882 00	3911.899 89	–3329.635 03	–113.688 62	–4344.550 61	5360.020 83	–5388.694 59
Mo	42	7.099 00	3986.076 87	–3933.481 96	890.586 42	–5056.546 74	5749.631 80	–5814.532 89
Tc	43	7.277 00	6393.170 19	–5663.102 89	–2553.070 43	–6103.538 93	15 489.398 23	–15 092.938 53
Ru	44	7.366 00	4158.681 68	–4368.321 69	3852.680 85	–15 204.139 05	19 803.188 91	–12 878.236 62
Rh	45	7.463 00	4042.882 10	–3955.924 19	–290.847 62	–3320.744 00	6712.897 01	–7702.333 42
Pd	46	8.336 00	4070.670 53	–3684.936 71	2649.012 57	–14 712.471 57	20 622.299 04	–12 632.888 84
Ag	47	7.576 00	3077.843 88	–2586.425 79	–3176.809 59	956.448 87	6241.018 66	–7460.849 83
Cd	48	8.993 00	6236.025 10	–5983.829 37	4089.974 73	–32 514.145 08	53 070.104 59	–31 768.842 56
In	49	5.786 00	3903.307 35	–3606.341 01	–1332.799 94	–5055.183 09	8807.433 32	–7155.155 11
Sn	50	7.343 00	5503.409 32	–4748.368 36	–3771.782 48	1167.057 84	531.790 26	–4334.964 85
Sb	51	8.641 00	7080.271 42	–6693.638 44	749.032 37	–15 155.106 88	21 478.593 04	–14 930.120 06
Te	52	9.009 00	7859.056 16	–7741.790 22	2571.568 46	–21 665.753 86	31 300.826 86	–21 158.955 03
I	53	10.456 00	9609.277 21	–9035.254 67	2276.900 29	–25 724.659 95	38 793.115 47	–26 591.847 26
Xe	54	12.129 00	9382.339 73	–8776.559 26	5345.283 32	–34 440.441 47	51 260.497 41	–31 421.339 05
Cs	55	3.894 00	1952.077 68	–1301.647 98	–3361.239 50	9846.506 47	–16 124.881 06	7299.096 96
Ba	56	5.211 00	6449.708 61	–5525.359 37	–2294.133 49	–3042.615 09	3370.700 75	–6035.642 98
La	57	5.750 00	7270.148 46	–6440.900 01	–1342.174 37	–6810.767 80	8722.682 61	–9490.439 50
Ce	58	5.620 00	6993.639 14	–6236.234 27	–1215.585 38	–7470.995 93	10 634.749 58	–10 693.747 18
Pr	59	5.460 00	6545.897 59	–5702.764 90	–1855.435 87	–4597.474 44	6296.622 31	–7985.799 70
Nd	60	5.490 00	6488.920 60	–5632.781 45	–2219.103 29	–3682.747 15	5715.268 23	–7957.133 85
Pm	61	5.550 00	6471.043 63	–5598.324 79	–2498.640 20	–3090.389 37	5459.135 39	–8040.676 17
Sm	62	5.600 00	6481.600 10	–5763.918 56	–1229.358 91	–7242.699 35	11 079.122 67	–10 747.091 03
Eu	63	5.660 00	6455.870 16	–5607.155 44	–2119.483 88	–5067.162 40	8955.603 33	–10 002.649 60

(*continues on next page*)

Table 1 (*Continued*).

Element	Z	E_i/eV	$10^{20}\,A_j$/m^2 (eV)^2	$10^{20}\,B_{j1}$/m^2 (eV)^2	$10^{20}\,B_{j2}$/m^2 (eV)^2	$10^{20}\,B_{j3}$/m^2 (eV)^2	$10^{20}\,B_{j4}$/m^2 (eV)^2	$10^{20}\,B_{j5}$/m^2 (eV)^2
Gd	64	6.160 00	7068.310 16	–7185.999 22	4764.075 44	–25 223.566 75	32 803.014 71	–20 557.038 88
Tb	65	5.980 00	6779.593 89	–7282.506 78	6775.292 89	–30 411.710 20	39 429.939 62	–23 545.499 59
Dy	66	5.800 00	6352.317 69	–5599.378 90	–1397.853 14	–69 68.662 54	11 586.455 77	–11 273.189 88
Ho	67	6.040 00	6525.944 04	–5797.113 04	–993.545 31	–7828.182 69	11 999.062 00	–11 269.831 55
Er	68	6.080 00	6482.318 16	–5797.617 64	–656.611 14	–8743.551 14	13 201.138 07	–11 815.745 80
Tm	69	6.160 00	6480.075 49	–5827.503 39	–255.035 88	–9749.331 62	14 266.916 24	–12 213.418 04
Yb	70	6.240 00	6477.234 51	–5840.815 65	37.307 29	–10 525.477 68	15 127.394 81	–12 543.838 34
Lu	71	6.150 00	5989.445 00	–6409.785 24	3039.489 57	–16 681.694 74	22 247.472 74	–15 149.023 03
Hf	72	7.000 00	6766.5480	–6572.443 65	2791.075 12	–17 448.724 38	21 112.937 88	–13 965.126 28
Ta	73	7.885 00	7529.245 00	–6574.155 17	–1793.780 65	–4301.404 32	3863.422 46	–6450.673 28
W	74	7.984 00	7842.451 00	–7527.342 67	2032.899 37	–15 922.818 44	19 876.442 28	–15 157.704 10
Re	75	7.876 00	7762.060 11	–7530.711 07	1078.805 37	–14 187.875 17	20 914.049 35	–17 366.225 12
Os	76	8.734 00	7092.471 01	–6468.102 87	–3122.659 78	1905.797 02	–576.486 92	–5857.632 86
Ir	77	9.298 00	7524.346 39	–6992.911 68	–2489.580 05	699.075 72	113.731 84	–6179.451 88
Pt	78	8.964 00	5712.967 74	–5935.958 67	6913.970 98	–27 401.936 45	35 723.026 16	–21 000.663 23
Au	79	9.225 00	4418.282 55	–4498.227 30	278.498 35	–79.570 92	–1439.609 20	–1816.319 07
Hg	80	10.437 00	7189.760 15	–6123.217 94	–7872.304 75	14 027.504 67	–11 728.383 45	–1584.890 54
Tl	81	6.108 00	4289.822 27	–4514.661 19	4060.751 11	–24 001.909 78	32 708.912 23	–17 298.719 71
Pb	82	7.416 00	5645.216 93	–5307.647 99	696.821 91	–14 334.976 06	19 122.787 62	–11 331.894 82
Bi	83	7.289 00	5949.211 11	–5956.751 20	23.087 28	–6865.551 50	6003.061 77	–5209.695 75
Po	84	8.428 00	7307.775 75	–6847.945 53	–2560.198 76	–532.621 63	–2286.759 24	–2132.789 50
At	85	9.600 00	8738.289 20	–7867.447 56	–4300.040 07	2924.155 66	–6791.403 52	–841.065 43
Rn	86	10.748 00	10 185.804 52	–8915.860 76	–5741.050 40	5245.761 90	–9640.257 70	–420.823 96
Fr	87	4.370 00	2404.437 80	–1908.645 95	–1574.130 66	3058.213 71	–8061.229 48	4078.120 27
Ra	88	5.279 00	6735.992 79	–6004.898 21	–348.676 89	–10 210.202 83	12 332.692 74	–9855.507 73
Ac	89	5.600 00	7489.848 38	–7649.496 94	3584.787 86	–18 677.029 36	21 202.934 79	–14 579.218 96
Th	90	6.000 00	8141.481 73	–7293.839 09	27.480 63	–13 366.939 99	17 839.970 62	–14 441.452 23
Pa	91	6.050 00	7968.433 85	–7388.288 34	1517.291 04	–16 771.917 62	21 224.619 17	–15 338.744 71
U	92	6.110 00	7916.665 08	–7174.739 62	–237.880 61	–11 575.037 75	15 358.906 44	–12 992.677 72
Np	93	6.150 00	7861.408 55	–7030.411 74	–1606.643 24	–8084.111 18	12 190.509 06	–12 060.881 77
Pu	94	5.800 00	7170.655 32	–6642.121 97	1150.389 81	–14 868.969 62	19 734.034 59	–14 581.716 12
Am	95	5.910 00	7478.803 13	–7146.267 12	2359.766 97	–22 360.968 47	32 782.684 83	–22 052.684 36

Experimental ionization efficiency curves published up to 1986 for atoms and molecular gases are reproduced in [145]. Measurements for 27 atoms were performed since with a crossed-beam apparatus based on the use of fast atoms and molecules rather than on thermally produced ones [146–149]. Results of earlier measurements for several additional elements are also cited in the latter reference. After reviewing their and prior experimental methods and making a detailed analysis of causes of error, overall uncertainties of respectively ±7 and ±15 % (one standard deviation) were evaluated for relative and absolute cross-sections [146]. Similar uncertainty limits (±5 to ±20 %) were ascribed to mass spectrometric determinations of electron impact cross-sections for formation of both positive and negative ions of C_{60} and C_{70} [150]. In crossed beam as well as in mass spectrometric experiments, part of the uncertainty in measured cross-sections is, especially at high temperature, due to the use of molecular beam sources for reasons discussed in Sections 4.4 to 4.8. In fast atom beams, the presence of excited states with long lifetimes may influence the results.

In Table 2, we compare the maximum ionization cross-sections, σ_m, calculated by Otvos and Stevenson (OS), by Gryzynski (G), and by Mann (M) with experimental values for the maximum cross-sections and for the corresponding energy. Also given are experimental cross-sections at E = 70 eV. Table 3 compares ratios of calculated (M) and experimental values. Using recent experimental values of $\sigma(E)$ for comparison with the four models described above, satisfactory agreement is found with Mann's calculations and Lotz' estimates. A typical comparison, that for Ag, is shown in Fig. 2. Some of the experimental and estimated values recommended by Lennon et al. [142], deviate appreciably from the calculated results. Figure 3 shows the extent of the discrepancies for elements with atomic numbers Z = 1 to 28. Although Mann's calculated cross-sections by and large agree with experimental data, significant disagreements exist. A possible reason is that excitation–autoionization processes [144] were not included in the calculations. In some cases, experimental error may also be indicated. Significant discrepancies are observed for Al, Ga, and In, with experimental [146] cross-sections 60 % larger than the calculated ones. For these elements, evidence for excitation–autoionization is summarized in [146]. Theoretical treatment including excitation–autoionization of Cr [151] yields cross-sections in good agreement with experimental data [152], that are appreciably higher than follows from formulae considering only direct ionization. For Cs [153] and Rb [154], the importance of excitation–autoionization is again borne out by theoretical calculations. For Zn, Cd, and Hg, the process was evidenced during determination of ionization efficiency curves near their thresholds [155].

Table 2 Maximum ionization cross-sections of atoms, σ_m; 1 Å^2 = 10^{-20} m^2.

	σ_m/Å^2 OS [134]	σ_m/Å^2 G [135]	σ_m/Å^2 M [139]	E_m/eV M [139]	E_m/eV exp	σ_m/Å^2 exp	σ_m/Å^2 exp	Ref.
H	0.33	0.76	0.22	37	51	0.63	0.61	[141] [156]
He	0.23	0.41	0.21	98	145	0.38	0.32	[146]
Li	2.8	3.3	3.29	15	15	4.29	1.90	[141]
Be	2.1	2.9	3.16	35		3.15	2.50	[141]
B	1.7	3.2	2.60	41	40	1.74		[141]
C	1.4	2.8	1.98	51		2.07	0.05	[141]
N	1.3	2.4	1.52	62		1.4		[141]
O	1.1	3.2	1.27	69		1.6		[141]
F	0.62	2.4	1.03	80	130	0.98	0.87	[147]
Ne	0.58	1.7	0.82	97	180	0.74	0.49	[146]
Ne								[157]
Na	4.8	3.8	4.02	14	100	10.50		[145]
Na				14	14	4.30	2.01	[158]

(*continues on next page*)

Table 2 (*Continued*).

	σ_m/Å^2 OS [134]	σ_m/Å^2 G [135]	σ_m/Å^2 M [139]	E_m/eV M [139]	E_m/eV exp	σ_m/Å^2 exp	σ_m/Å^2 exp	Ref.
Mg	5.3	4.0	5.38	29	20	5.30	3.07	[149]
					17	5.47	2.95	[159]
Al	5.1	4.9	6.18	31	24	9.90	7.82	[149]
Si	4.8	4.9	5.35	37	27	6.69	5.87	[149]
P	4.6	4.4	4.45	45	36	5.26	4.91	[149]
S	4.3	5.5	3.87	51	36	4.50	4.41	[149]
Cl	3.9	4.5	3.40	57	62	3.49	3.47	[147]
Ar	3.6	3.7	2.83	67	85	2.62	2.65	[146]
					85	2.55	2.49	[160]
					85	2.70	2.67	[161]
K	12.9	5.6	7.21	12			5.9	
Ca	14.0	6.0	10.44	23	29	7.8		[162]
Sc	12.7	6.9	9.51	25				
Ti	12.2	7.8	8.67	27			8.7	[149]
V	11.9	8.6	7.93	29			7.2	[149]
Cr	9.3	10.9	5.10	24	29	8.9	7.5	[152]
Mn	10.0	11.8	6.75	33				
Fe	9.3	13.0	6.30	35	29	5.34	4.38	[149]
						5.4	4.4	[152]
					26	4.01	3.29	[163]
Co	8.7	12.9	5.96	36			5.87	[149]
Ni	8.1	14.3	5.48	39			5.04	[149]
Cu	6.1	12.9	3.80	31	27	4.09	3.47	[149]
Cu					30	3.21	2.89	[164]
Zn	5.3	7.9	4.65	44	50	5	5.03	[149]
Ga	6.0	7.3	5.94	41	34	9.19	8.26	[149]
					27	11.0	8.49	[165]
Ge	6.1	5.8	5.71	47	32	7.46	6.64	[149]
As	6.2	5.0	5.02	45	40	6.12	5.69	[149]
Se	6.1	6.0	4.96	47	45	5.90	5.73	[149]
Br	6.0	5.3	4.55	52	50	4.43	4.36	[147]
Kr	5.8	4.7	4.05	61	70	3.70	3.70	[146]
Rb	19.4	6.5	8.40	11			6.8	[145]
Sr	21.4	7.0	12.91	22	6.0			
Y	19.8	6.0	11.91	25				
Zr	19.9	8.8	10.87	27				
Nb	19.2	11.6	7.74	23				
Mo	17.5		6.91	27				
Tc	16.0		9.13	32				
Ru	14.7		6.73	28				
Rh	13.5		6.17	30				
Pd	8.4		6.07	32				
Ag	11.6	11.4	5.05	37	45	5.47	5.21	[149]
Cd	7.3		6.29	47			8.54	[149]
In	8.3		7.72	45	27	12.17	9.91	[149]
Sn	8.6	7.9	7.70	49	30	9.77	8.42	[149]
Sb	8.7		7.19	55	32	8.32	7.40	[149]
Te	8.5		7.09	42	45	8.27	7.92	[149]

(*continues on next page*)

Table 2 (*Continued*).

	σ_m/Å^2 OS [134]	σ_m/Å^2 G [135]	σ_m/Å^2 M [139]	E_m/eV M [139]	E_m/eV exp	σ_m/Å^2 exp	σ_m/Å^2 exp	Ref.
I			6.75	47	40	6.03	5.91	[147]
Xe	8.0	6.0	6.24	53	40	4.80	5.35	[146]
Cs	24.4	8.4	10.78	11	(15)	(10)	(8)	
Ba	26.0		17.26	31	(15)	(14)	(6)	
La			16.07	34				
Ce			15.91	22				
Pr			16.01	32				
Nd			15.63	21				
Pm			15.24	22				
Sm			14.88	22				
Eu			14.60	23				
Gd			12.92	35				
Tb			12.73	27				
Dy			13.90	23				
Ho			13.42	24				
Er			13.20	24				
Tm			12.99	24				
Yb			12.77	24				
Lu			10.92	31				
Hf			10.44	33				
Ta			9.55	37				
W			9.24	32				
Re			9.05	33				
Os			8.09	38				
Ir			7.71	40				
Pt			6.60	34				
Au		12.4	5.85	39	86.00	5.70	5.50	[152]
Hg	9.1	9.8	6.43	50	100.00		9.40	[149]
Tl	10.0		7.76	48	100.00	7.00	6.50	[145]
Pb	10.4		7.85	52	32.00	8.32	7.27	[149]
						7.41	5.86	[166]
Bi			8.12	54	40.00	8.76	8.01	[149]
Po			7.91	58				
At			7.61	63				
Rn			7.29	68				
Fr			10.21	29				
Ra			17.52	32				
Ac			16.51	36				
Th			16.74	31				
Pa			16.22	32				
U	18.5		15.87	32	25.00		7.66	[149]
Np			15.38	33				
Pu			15.83	30				
Am			14.80	34				

Table 3 Relative ionization cross-sections of atoms $\sigma(E; A^+/A)/\sigma(E; B^+/B)$.

A	$\sigma(E; A)/Å^2$ [a]	*B*	$\sigma(E; A)/Å^2$ [a]	*E*/eV	$\sigma(E; A^+/A)/\sigma(E; B^+/B)$ exp[b]	Ref.
Cd	6.06	**Ag**	4.59	70	0.80[c]	[202]
Cu	3.23	**Ag**	4.59	70	0.65[c]	[202]
Pb	7.67	**Ag**	4.59	70	1.27[c]	[202]
Zn	4.43	**Ag**	4.49	70	0.58[c]	[202]
Ti	8.47	**Ag**	4.31	21	1.75	[194]
V	7.52	**Ag**	4.16	20	1.59[c]	[20]
Al	6.13	**Ag**	5.05	37	2.66[c]	[267]
Si	5.35	**Ag**	5.05	37	1.64[c]	[267]
Ag	4.93	**Pb**	7.85	50	0.81[d,e]	[268]
Tl	7.76	**Ca**	9.70	50	1.10[d,f]	[268]
Ag	4.93	**Ca**	9.70	50	0.63[d,f]	[268]
Ti	8.38	**B**	2.60	40	7.6[g]	[269]
Gd	12.50	**S**	4.93	20	4.35[g]	[270]
Eu	14.53	**S**	2.54	20	3.52[g]	[94]
Mn	4.57	**Se**	1.99	14	2.4[g]	[271]
Mn	6.11	**Te**	3.43	20	1.20[g]	[272]
Pt	6.11	**Ag**	4.77	60	1.87[h]	[273]
Au	5.60	**Ag**	4.77	60	1.27[h]	[273]
Ti	8.13	**V**	4.31	18	1.0[i]	[206]
Ti	8.13	**Cr**	7.24	18	0.89[i]	[206]
V	7.24	**Cr**	4.93	18	0.64[i]	[206]
Cu	2.89	**In**	5.81	16.5	0.74[i]	[207]
Ni	3.76	**Fe**	4.84	(16.5)[m]	0.21[i]	[207]
Co	4.45	**Fe**	4.84	(16.5)[m]	0.60[i]	[207]
Al	5.25	**Fe**	4.84	(16.5)[m]	1.60[i]	[207]
Cu	2.89	**Ag**	3.33	(16.5)[m]	0.85–1.07[i]	[207]
Cu	2.89	**Au**	3.64	(16.5)[m]	1.8–2.10[i]	[207]
Ag	3.33	**Au**	3.64	(16.5)[m]	1.2–1.45[i]	[207]
Cu	2.89	**Au**	3.64	(16.5)[m]	1.09[j]	[207]
Cu	2.89	**Au**	3.64	(16.5)[m]	1.6[k]	[207]
Cu	2.89	**Au**	3.64	(16.5)[m]	1.54[l]	[207]

[a]See also ref [149]; 1 $Å^2 = 10^{-20}$ m^2.
[b]See Section 6.5.
[c]From relative integrated intensities.
[d]In crossed beams.
[e]$\sigma(\text{total}, Ag^{n+})/\sigma(\text{total}, Pb^{n+}) = 0.70$.
[f]$\sigma(\text{total}, A^{n+})/\sigma(\text{total}, B^{n+})$.
[g]From relative intensities and pressures at congruency.
[h]From intensities and vapor pressures at the melting points.
[i]By extrapolation to unit activity in the alloy and use of vapor pressures for the standard states of the elements.
[j]In Cu–Au–Sn alloys.
[k]in Cu–Au–Ge alloys.
[l]In Cu–Au–In alloys.
[m]Assumed here.

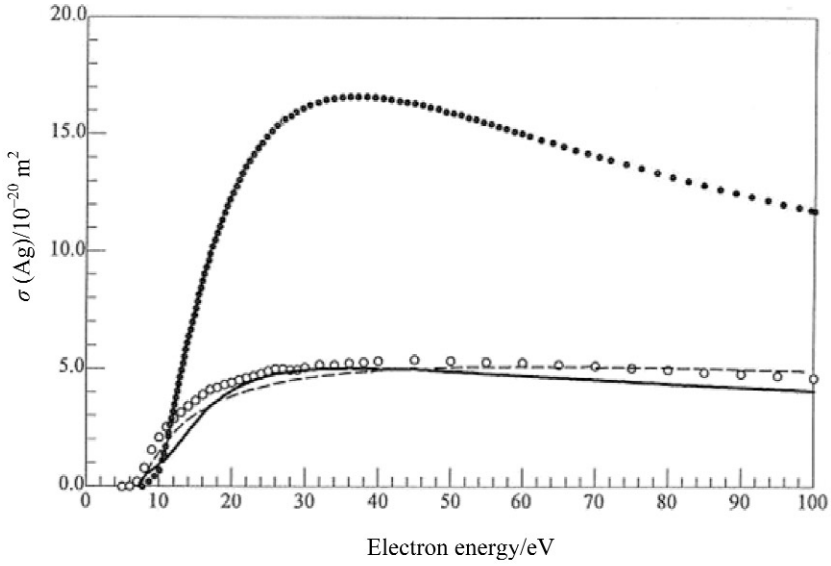

Fig. 2 Energy dependence of the ionization cross-section of Ag. Experimental results [149] o; Calculated data from: Gryzinski [135]; Lotz [137] dashed line; Mann [139] heavy line.

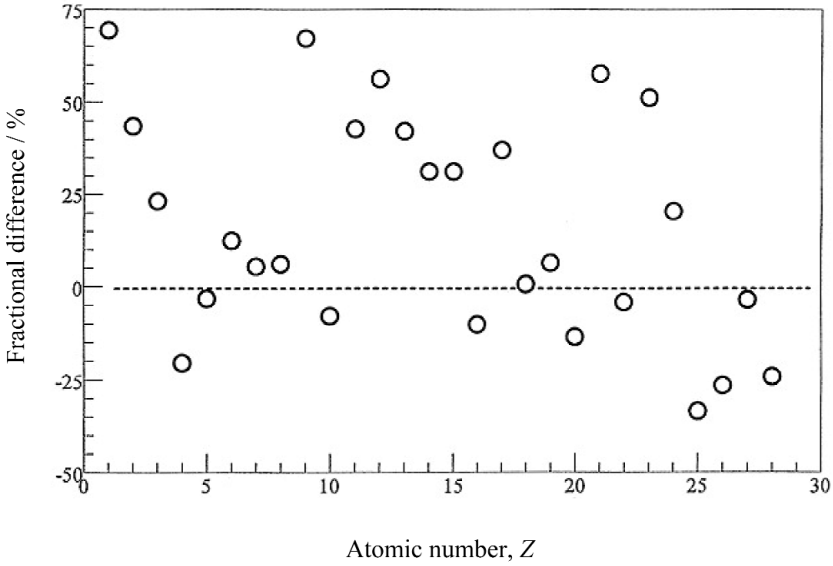

Fig. 3 Fractional difference $\Delta\sigma_m/\sigma_m$ between assessed experimental ionization cross-sections at their maxima [141,142] and the corresponding values calculated by Mann [143] for elements 1(H) to 28(Ni).

A pulsed cross-beam technique incorporating time of flight spectroscopy [156–166] or related experimental procedures has been used since in additional studies of the ionization of several atoms.

In mass spectrometric investigations at high temperatures, ionization cross-sections of the elements calculated by Mann [138,139] are generally used. Early studies relied on calculated maximum ionization cross-sections [134,138]. Quasi-linear variation of the ionization cross-section, or of the ionization efficiency curve, $\sigma(E_j) \approx \sigma(E_m)(E - E_i)/(E_m - E_i)$, in the entire interval [9] between E_i, the ionization energy of the species considered and E_m, rather than close to E_i only [4] has been found [18] to lead to significant deviations where tested.

In order to perform semi-empirical calculations of ionization cross-sections for molecules (see below), Gryzinski's formula was modified [167,168] by replacing the first constant by the square of the orbital radii [140] and by introducing orbital weighting factors [169].

6.3 Ionization cross-sections of molecules

In keeping with the physical and physicochemical interpretation of the behavior of molecules upon interaction with electrons or photons [98–118], it is accepted here that ionization of molecules may be described as follows:

$$\begin{aligned}
&e^- + M_j \rightarrow M_j^{\bullet +} + 2e^- \ [\sigma(M_j^{\bullet +})], \text{ transition state} \\
&M_j^{\bullet +} \rightarrow M_1^+ \ [\sigma(M_1^+/M), I_1^+] \\
&M_j^{\bullet +} \rightarrow M_2^+ \ [\sigma(M_2^+/M), I_2^+] \\
&\text{etc.....} \\
&M_j^{\bullet +} \rightarrow M_n^+ \ [\sigma(M_n^+/M), I_n^+]
\end{aligned} \tag{18}$$

with

$$\sigma(M_j^+) \geq \sum_k^n \sigma(M_k^+) \tag{19}$$

The transition state $M_j^{\bullet +}$ is an excited and metastable intermediate ionic state or set of states, whose too short lifetime(s) in general preclude detection [116–118]. M_j^+ represents the parent and fragment ions of the species M_j being ionized. If sufficiently abundant, account should be taken of multiply charged ions. Production of negative ions by electron attachment or by ion pair formation from excited neutral states produced by electron impact, are not considered in the present context. Such processes indeed take place in limited energy ranges and with other threshold laws [112–115].

Relation 1 between the partial pressure of the gaseous species M_j and the various ion intensities, may now be written as:

$$p(M_j) = I_1^+ \ T/S_1 = I_2^+ \ T/S_2 = ... = I_n^+ \ T/S_n \tag{20}$$

with

$$S_j = \sum_{k=1}^n S_k = g \sum_{k=1}^n \sigma_k \gamma_k f_k \tag{21}$$

Combining these relations, one obtains:

$$\sigma(M_j) = \frac{S_1}{g\gamma_1 f_1}\left[1 + \frac{I_2\gamma_1 f_1}{I_1\gamma_2 f_2} + ... + \frac{I_n\gamma_1 f_1}{I_1\gamma_n f_n}\right] \tag{22}$$

As a summation principle is applied with respect to the total ionization cross-section $\sigma(M_j^+)$ (see step 1 in 18), at least the main features of the fragmentation pattern should be identified and all ion intensities measured simultaneously during vaporization experiments.

The additivity rule, i.e., the assumption that summing ionization cross-sections of the constituent atoms provides an approximation to the ionization cross-section of a molecule, was suggested by Otvos and Stevenson [134]. These authors

- drew attention, as mentioned earlier, to Bethe's result that the ionization cross-section of an atomic electron is approximately proportional to the mean square radius of the shell it occupies;

- calculated relative ionization cross-sections with hydrogen-like wave functions for the majority of the elements;
- showed that, for a variety of hydrocarbons and inorganic gases, the cross-sections for ionization by a single electron accelerated to ca. 75 eV in different types of sources support the additivity postulate; and
- noted that the correlation remains valid for ion production by high-energy β particles.

Measurement of ionization cross-sections for increasingly large numbers of organic molecules and inorganic gases, and their statistical treatment [170–173], showed that

- the Otvos and Stevenson additivity postulate is not vitiated by differences in the tendency of organic molecules to undergo neutral dissociation rather than ionization upon collision with electrons;
- total molecular cross-sections for ionization should be viewed as linear rather than strictly additive combinations of atomic cross-sections;
- the average contribution of a given atom to the total cross-section of a molecule is quite close to the maximum atomic cross-section calculated for that atom by Mann [138];
- molecular cross-sections for ionization are lowered in the presence of fluorine as a hetero-atom, and grow smaller as the number of chlorine atoms increases in the molecule; and
- there are indications for the carbon atom contribution to depend on its bonding configuration.

The above data treatment was extended to include P, As, B, and Si atoms, was used to confirm a "fluorine anomaly" [171,174–176], and served to derive empirical correction factors for previous supposedly additive cross-sections. Figure 1 in ref. [175] shows that the anomaly extends to atoms with $Z = 7$ to 15 (N to Si).

For diatomic molecules, such as H_2, N_2, O_2, S_2, Se_2, Te_2, and dimeric alkali halides, review of early measurements [5,8] had already shown that the cross-section is but ca. 50 % higher than for the atom or the monomer, rather than twice as large. Comparable deviations were observed for hetero-nuclear high-temperature molecules. For the magnesium dihalides [177] as for a number of organic molecules [171,178], a correlation between cross-sections and polarizabilities was noted.

Many of the deviations from additivity can be rationalized by noting that most formulae for calculating atomic cross-sections are functions of the number of equivalent electrons, their quantum number and binding energy in a given orbital, the nature of which may also determine the energy dependence of the orbital's contribution to the total cross-section. Alterations in the orbital or in any of its properties between the atom and the molecule are, therefore, likely to cause deviations from simple additivity rules. In addition, cross-sections calculated for atoms do not usually take into account excitation–autoionization and other factors that are more likely to change than to remain constant upon molecule formation.

Recent efforts concern the quantification of these factors in molecules. The modified Gryzinski–Binary Encounter model for atoms [167,168] is the basis for an additivity rule with atomic weighting factors calculated from a Mulliken analysis of the molecular orbital populations [179] and explains [180] why $\sigma_{SiF} > \sigma_{SiF_2} > \sigma_{SiF_3}$.

A modified additivity rule [181], viz.:

$$\sigma[(AB_n)^+] = f_A(r_A, N'_A; r_B N'_B)\sigma[(A)^+] + f_B(r_A, N'_A; r_B N'_B)n\sigma[(B)^+] \quad (23)$$

has been proposed in terms of the ionization cross-section for atoms and of atomic weighting factors given by:

$$f_A(r_A, N'_A; r_B, N'_B) = [(\pi r_A^2)/(\pi r_B^2)]^{1/2}[N'_A/(N'_A + nN'_B)] \quad (24)$$

$$f_B(r_A, N'_A; r_B, N'_B) = [(n\pi r_B^2)/(\pi r_A^2)]^{1/2}[nN'_B/(N'_A + nN'_B)] \quad (25)$$

r refers to the quantum theoretically calculated radius [140] of the outermost orbital in the atom (A or B) and N' to the atom's effective number of electrons in the molecule as obtained by Mulliken population analysis. These concepts have been developed and applied to various molecules with experimentally known cross-sections (182).

Bobeldijk et al. [183] ascribe deviations from the additivity rule to mutual shielding of atoms or groups of atoms. A corollary is that the ionization cross-section depends on the orientation of the molecule relative to the impinging electron beam. The observed cross-section is consequently an average over end-on and broadside contributions. To reduce the propagation of deviations from atoms to molecules, ionization cross-sections of the latter are calculated from those of atomic aggregates.

A theoretical model initially free of adjustable or fitted parameters has been developed by Kim and Rudd [184] to calculate electron-impact ionization cross-sections for atoms and molecules. This approach takes into account that electron-atom collisions are of two general types:

- soft or distant collisions having large impact parameters due to dipole interaction between the incident particle and the target;
- hard or close collisions described by the Mott or binary encounter (BE) theory.

The resulting BED model combines the latter and the description of dipole interaction with fast incident electrons in the Bethe theory. The number of ab initio molecular parameters required is reduced in a simplified version of the theory, the binary encounter-Bethe or BEB model [185].

The data required are: the binding energy B (i.e., $-E_i$, the negative of the ionization energy) and the average kinetic energy U for the electrons in each orbital in the initial state of the target atom or molecule. The wave functions for both the initial and the final state are needed to calculate the continuum dipole oscillator strength df/dW, W being the energy of the ejected electron. The binding and the kinetic energies, B and U, are evaluated in atomic or molecular wave function codes that calculate total energies. The binding energy B may be (and preferably is [184]) replaced by the experimental value. Unless the oscillator strength df/dW can be deduced from experimental photo-ionization cross-sections, its calculation may be a limiting factor in the BED model. Where that is the case, the BEB model is an approximation using a simplified representation for df/dW.

A synoptic discussion of oscillator strength distribution in (photo)-ionization is, for example, given by Berkowitz in [102]. The relation between sum rules for the number of electrons in the system and the photo-absorption cross-section are illustrated there for atoms and a variety of molecules. It is further shown that ionization is generally a more important process than molecular bond rupture. Both processes may, however, be competitive when absorption of photons (or as here, energy transfer by the impinging electrons) leads to a quasi-discrete neutral state. The rates of interaction with ionic and neutral continua determine whether autoionization or molecular dissociation is more pronounced.

In the BED model, the cross-section for ejecting an electron from a given subshell is:

$$\sigma_{\mathrm{BED}}(t) = \frac{S}{t+u+1}\left[D(t)\ln t + \left(2 - \frac{N_w}{N}\right)\left(\frac{t-1}{t} - \frac{\ln t}{t+1}\right)\right] \tag{26}$$

with

$$D(t) = N^{-1}\int_0^{(t-1)/2} \frac{1}{w+1}\frac{\mathrm{d}f(w)}{\mathrm{d}w}\,\mathrm{d}w \tag{27}$$

and

$$N_w \equiv \int_0^{\infty} \frac{\mathrm{d}f(w)}{\mathrm{d}w}\,\mathrm{d}w \tag{28}$$

where $t = T/B$, T being the kinetic energy of the impacting electron, $u = U/B$, $w = W/B$, N the number of bound electrons in the subshell, $S = 4\,\pi\,a_0^2\,NR_y^2/B^2$, with $a_0 = 0.5292 \times 10^{-10}$ m and $R_y = 13.61$ eV.

In the BEB model, $df/dW = N/(w + 1)^2$ is assumed, giving the integrated cross-section per orbital as:

$$\sigma_{\mathrm{BEB}}(t) = \frac{S}{t+u+1}\left[\frac{\ln t}{2}\left(1-\frac{1}{t^2}\right)+1-\frac{1}{t}-\frac{\ln t}{t+1}\right] \tag{29}$$

Total ionization cross-sections are obtained by summing the orbital σ's from each subshell.

For fitting purposes, simplified versions of the BEB-formula (eq. 29) may be used. These are obtained by omitting summation over subshells and the term in u, and by using the lowest binding energy B to define the single term in t.

A general analytical formula [186] describes the variation of the ionization cross-section σ_j for species j with the energy E of various charged projectiles in terms of the threshold energy E_{i} for ionization of the target, the energy E_{m} for which σ_j reaches its maximum, and an exponent, a_i, that depends on the charge of the projectile and its mass relative to that of the target. The excess energy should, however, be uniquely defined, i.e., the cross-section should be dominated by removal of an electron from a single orbital.

When the ionizing projectile is an electron, $a_i = 1.127$ and the general formula takes the form:

$$\frac{\sigma(E)}{\sigma(E_{\mathrm{m}})} = \frac{3.8612\,z^{1.127}}{(0.8873+z)^{2.127}} \tag{30}$$

where $z = (E - E_{\mathrm{i}})/(E_{\mathrm{m}} - E_{\mathrm{i}})$.

Another recent model free of adjustable parameters is based on a subtle combination of quantum-chemical and classical concepts [187]. It postulates ionization to occur when the Coulomb potential experienced by a molecule in the electric field of an approaching electron, viewed as a point charge, equals the ionization energy. Ab initio calculations provide the distance between the electron and the center of mass of the molecule that is required to meet this condition. This distance r (if necessary, averaged over different angles of approach) is considered to yield the maximum collision cross-section $\pi\,r^2$. The corresponding energy follows from the assumption that coupling with the incoming wave is strongest when its frequency equals that of an electron orbiting on a classical circular trajectory of radius r.

Transfer of an electron from an orbital with a large radius to an orbital with a small one, as in formally ionic molecules, would immediately lead to ionization cross-sections less than expected by additivity. An examination of possible correlations between predicted and observed cross-sections and Pauling electronegativities [188] might, therefore, be useful. No systematic or quantitative rule can, however, be deduced at present, because distortion of orbitals upon molecule formation cannot be simply evaluated.

In a number of instances, the ionization energy is lower for the molecule than for one or more of the constituent atoms. Rigorous application of the additivity rule at intermediate energies would then entail that the atoms with the higher ionization energy do not contribute to the cross-section, while Mulliken population analysis may, on the contrary, show their orbital occupancy to be increased. It is suggested that the ionization cross-section of the molecule then be estimated with relation 30 (or another of the preceding ones) after adding the cross-sections of the atoms at or in the vicinity of their maxima. Qualitative correlation between the united and the separated atoms [189] actually already implies that the atom with the higher E_{i} (lower energy in such diagrams) acquires an increased electron population in the molecule.

6.4 Partial ionization cross-sections of molecules

For HTMS applications, the partial cross-section for production of the singly charged parent ion $\sigma(A^+/A)$, is generally more useful than the total ionization cross-section, especially in polyatomic molecules, where elucidation of the full fragmentation pattern is not always possible. There may also be cases where it is advantageous to base a pressure determination on intensity measurements for a fragment ion. Partial cross-sections are influenced by several parameters:

- Frank–Condon factors for transitions between the neutral molecule and the ground state and to those electronically excited states of the ion that are accessible at the energy of the impacting electron;
- transition probabilities to the mentioned states of the ion as a joint function of the internal energy present in the neutral molecule and of the kinetic energy of the colliding electron; and
- stabilities of the individual states of the ion toward decomposition.

Generalizations made on the basis of the partial cross-section ratios given in Tables 4 and 5 are [20]:

$$\sigma(M_2^+/M_2)/\sigma(M^+/M) = 1.80 \pm 0.20 \text{ for homonuclear molecules} \quad (31)$$

$$\sigma(A_2B_2^+/A_2B_2)/\sigma(AB^+/AB) = 1.25 \pm 0.35 \text{ for dimeric molecules} \quad (32)$$

$$\sigma(MO^+/MO)/\sigma(M^+/M) = 0.65 \pm 0.10 \text{ for monoxides} \quad (33)$$

$$\sigma(MO_2^+/MO_2)/\sigma(MO^+/MO) = 0.50 \pm 0.25 \text{ for dioxides} \quad (34)$$

all at energies a few eV above the ionization energy. For the monoxides referred to, the ionization energy only slightly exceeds that of the metal atoms. For the dioxides, it is 2 to 3 eV higher.

Although it is clear that more information is required, especially for polyatomic high-temperature molecules, a tentative generalization is that the ionization potential reflects the number of electrons not involved in chemical bonding and thereby provides hints with respect to whether the total ionization cross-section would be high or low in comparison with the value predicted by additivity. Experimental values for W_2O_6 and W_3O_9 are in line with those for UO_3 with a lower ionization cross-section than UO and UO_2 (channel $UO_3 + e^- \rightarrow UO_3^+ + 2e^-$) [190].

Comparison of experimental cross-sections with those for the corresponding united atoms or truncated united atoms shows no generally valid, even approximate, agreement. It should also be noted that the above average cross-section ratios imply approximate constancy of the degree of dissociative ionization in the molecules considered. Caution is indicated when using these ratios (or other constant ones) for whole groups of molecules, e.g., the halides for which the relative importance of dissociative ionization apparently varies appreciably as a function of the electronic structure of the metal as well as of the nature of the halogen [11].

Table 4 Relative ionization cross-sections of diatomic molecules[a].

AB	E_i(AB)/eV	A	E_i(A)/eV	E/eV	$\sigma(AB^+/AB)/\sigma(A^+/A)$	Ref.
H_2	15.43	**H**	13.60		1.44	[8]
H_2	15.43	**Ar**	15.76	30	0.29	[18]
N_2	15.58	**N**	14.53		1.93	[8]
N_2	15.58	**Ar**	15.76	30	0.57	[18]
N_2	15.58	**Ag**	7.58	40	0.26	[267]
O_2	12.08	**O**	13.62		1.80	[8]
O_2	12.08	**Ar**	15.76	30	0.48	[18]
S_2	9.36	**S**	10.36		1.44	[8]
S_2	9.36	**S**	10.36	14	1.95	[20]
S_2	9.36	**S**	10.36	20	1.68	[20]
S_2	9.4	**Kr**	14	40	1.5	[274]
Se_2	8.88	**Se**	9.75		1.64	[8]
Se_2	8.88	**Se**	9.75	14	2.0	[20]
Se_2		**Cd**	8.99	20	2.1 ± 0.4	[275]
Te_2	8.29	**Te**	9.01		1.68	[8]
Te_2	8.29	**Te**	9.01	20	1.94	[268]
Te_2	8.29	**SiTe**			1.4	[8]
Ag_2		**Ag**	7.58	46	1.53	[132]
BaO	6.9	**TiO**	6.7	30	0.26	[93]
SiO		**Ag**	7.58	30	1.4 ± 0.2	[204]
TiO	6.7	**Ti**	6.82	22	0.85	[20]
ZrO	6.5	**ZrO_2**	9.5	11	6.4	[276]
VO	7.4	**V**	6.74	20	0.55	[20]
YO		**Y**	6.22		0.68	[8]
LaO		**La**	5.58		0.60	[8]
CeO	5.2	**Ce**	5.47	12	0.69	[20]
ThO	6.1	**Th**	6.11	12	0.74	[20]
UO	4.7	**U**	6.19	18	1.2	[278]
GdS	6.9	**Gd**	6.16	20	0.84	[20]
US		**U**	6.19	50	1.16	[8]
PbS	8.6	**Pb**	7.42	20	0.83	[20]
PbSe	8.4	**Pb**	7.42	20	1.03	[20]
PbTe	8.3	**Pb**	7.42	20	1.46	[20]
HCl	12.74	**Ar**	15.76	30	0.88	[18]
LiF	11.3	**N_2**	15.58	26	0.7	[125]
NaCl	8.9	**Ar**	15.76	30	0.38	[18]
KCl	8.4	**NaCl**	8.9	23	1.03	[20]
KCl	8.4	**Ar**	15.76	30	0.28	[18]
CsCl		**Ar**	15.76	30	1.19	[18]
CsI	6.5	**Li**	5.39	50	2.4	[277]
GaCl	10.1			26	2.05[a]	[279]
SiF	7.3			29	4.41[a]	[280]
GeCl	7.2			50	4.35[a]	[279]
SnCl	6.8			28	3.67[a]	[279]

[a]$\sigma(AB^+/AB)/10^{-20}$ m^2 (last 4 entries in column 6).

Table 5 Relative ionization cross-sections of polyatomic molecules.

AB	E_i (A_nB_m)/eV	A	E_i (A)/eV	E/eV	$\sigma(A_nB_m^+/A_nB_m)/\sigma(A^+/A)$	Ref.
C_{60}	7.61 ± 0.2	Ag		38	53.5 ± 5.6[a]	[195]
				100	24.6[a]	[150]
		Pb		48	80[a]	[197]
C_{70}	7.61 ± 0.1	Ag		38	54.5[a] ± 1.5	[196]
				100	19.3[a]	[150]
		Pb		48	80[a]	[197]
P_4		P_2		85	2.2	[281]
As_4		As_2		100	2.1	[281]
As_4		Cd		20	1.85	[275]
S_6	9.16	S_2	9.36	14	0.71	[8]
S_7	8.67	S_2	9.36	14	0.59	[8]
S_8	9.43	S_2	9.36	14	1.0	[8]
Se_5	9.1	Se_2	8.88	45	1.3[b]	[20]
Se_6	9.2	Se_2	8.88	45	0.36	[20]
Se_7	8.9	Se_2	8.88	45	0.35	[20]
H_2O	12.61	Ar	15.76	30	0.58	[18]
Li_2O	6.8	Li	5.39		0.63	[8]
Ga_2O		O_2		35[c]	6.9	[282]
In_2O	8.4	O_2	12.08	23	3.7	[20]
In_2O	8.4	In	5.79	23	2.1[b]	[20]
SO_2	12.34	Ar	15.76	30	0.50	[18]
TiO_2	9.0	TiO	6.7	70	0.45[d]	[20]
ZrO_2	9.5	ZrO	6.5	11	0.16	[276]
VO_2	9.6	VO	7.4	20	0.33	[20]
CeO_2	10.0	CeO	5.2	10.5	0.05[b]	[20]
ThO_2	8.7	ThO	6.1	12	0.19[b]	[20]
ThO_2	8.7	ThO	6.1	14	0.3[b]	[20]
UO_2	5.1	UO	5.7		0.8	[8]
UO_2	5.5	UO	4.7	20	0.32	[276]
UO_3	10.6	U	6.19	25	0.16	[276]
UO_3		UO_2		70	0.33	[190]
As_4O_6		Ar	15.76	30	20.77[d]	[18]
W_2O_6		Ag		50	2.4[d]	[268]
W_3O_9		W_2O_6		50	1.25[d]	[268]
BS_2		Zn	9.39		0.67	[8]
B_2S_2		Zn	9.39		2.0	[8]
B_2S_3		Zn	9.39		2.0	[8]
In_2S	7.6	S_2	9.36		0.83	[283]
In_2Se	7.5	Se_2	8.88		1.13	[283]
Li_2Cl_2		LiCl	10.1		1.15	[8]
Li_2Cl_2		LiCl	10.1		0.83	[8]
Li_2Br_2		LiBr	9.4		1.42	[8]
Li_2Br_2		LiBr	9.4		1.84	[8]
Li_2I_2		LiI	8.6		1.04	[8]
Na_2F_2		NaF			1.24	[8]
Na_2Cl_2	10.3	NaCl	8.9		1.58	[8]
Na_2Cl_2	10.3	NaCl	8.9	23	1.18[b]	[20]
Na_2I_2		NaI	7.64		0.86	[8]
K_2F_2		KF			1.27	[8]

(*continues on next page*)

Table 5 (*Continued*).

AB	E_i (A_nB_m)/eV	A	E_i (A)/eV	*E*/eV	σ ($A_nB_m^+/A_nB_m$)/ σ (A^+/A)	Ref.
K_2Cl_2	9.6	**KCl**	8.9		1.57	[8]
K_2Cl_2	9.6	**NaCl**	8.9	22	1.51[b]	[20]
K_2Cl_2	9.6	**KCl**	8.4	30	0.74[d]	[20]
SiF_2	11.2		14.0	35	1.50[a]	[284]
SiF_3	9.2		14.0	36	0.72[a]	[285]
K_2I_2			8.2		1.66	[8]
Rb_2Cl_2		**RbCl**			1.43	[8]
KNaCl		**NaCl**	8.9	22	1.30[b]	[20]
ZrF_4		**NaF**			0.56	[8]
ZrF_4		**NaF**			1.8	[286]
$NaZrF_4$		**NaF**			0.40	[8]
$NaZrF_5$		**NaF**			2.5	[286]
$NaScF_4$		**NaF**			2.1	[286]
VF_3		**NaF**			1.46	[286]
$NaVF_4$		**NaF**			1.5	[286]
NaV_2F_7		**NaF**			1.8	[286]
$NaZrF_5$		**NaF**			2.5	[286]
KOH	7.5	**Ar**	15.76	30	1.04	[18]
$(KOH)_2$	7.8	**KOH**	7.5	30	1.33[d]	[20]
$NaBO_2$	9.2	**KF**	(9.3)		1.4	[20]
$NaBO_2$	9.2	**NaF**			2.01 ± 0.1	[286]
KBO_2	8.6	**NaF**	(10.8)		1.5	[20]
KBO_2		**KF**			1.4 ± 0.1	[286]
$RbBO_2$		**RbF**			1.5 ± 0.1	[286]
$NaScF_4$		**NaF**			2.1	[287]
$NaVF_4$		**NaF**			1.5	[287]
NaV_2F_7		**NaF**			1.8	[287]
$(KReO_4)_2$		**$KReO_4$**			0.68	[8]

[a]Value in 10^{-20} m^2.
[b]Sensitivity ratio.
[c]*E*/eV = 35 for Ga_2O, 55 for O_2.
[d]Total cross-section.

6.5 Temperature dependence of partial ionization cross-sections

As expected [5] by analogy with organic molecules, temperature dependence of ionization processes has been observed at high temperatures for atoms, e.g., U [12], for diatomic molecules, e.g., I_2 [119], NaCl, KCl [18], CsCl [120], LiF [125], and for poly-atomic molecules, e.g., Ag_3Cl_3 [121] and As_4O_6 [20,122,123].

For diatomic molecules, modeling of the observations has been based on potential energy curves and modification of transition probabilities to the bound and repulsive parts of the potential energy curve in the molecular ion as a function of the vibrational levels in the neutral molecule and of their degree of occupation, which depends on temperature (Boltzmann factor). For polyatomic molecules, the quasi-equilibrium or statistical theory of mass spectra has been applied with different degrees of sophistication to discuss the observations in terms of thermal energy transfer during the ionization process and its randomization with the energy deposited in the molecule by the impacting electron [123].

In supersonic molecular beam sampling [15], dynamic effects in expanding gases need to be considered. For cross-section determinations, or their use in converting mass spectral ion intensities into

partial pressures, the most significant effects are expansion cooling, velocity enhancement, and radial diffusion. One result of these phenomena is that the instrument sensitivity factor g changes slightly as either source pressure or temperature are modified. While these effects can be quantified, their incidence during determination of cross-sections and pressures can be reduced through use of reference vapor species with molecular weights and heat capacity ratios ($\gamma = C_p/C_v$) similar to those of the species under investigation.

Several advantages are inherent to the SMBS approach. First, the pulsed nature of the molecular beam, prior to its MS detection, allows determination of velocity and of postexpansion temperature [191]. As these beam quantities are related to molecular weights, the latter can be determined independently of MS detection. Incorrect mass spectral assignment of ions to their molecular precursors can so be avoided. The often dramatic beam cooling (a factor of 10 or more) that accompanies SMBS can lead to electron impact mass spectral patterns that differ markedly [125] from those found in classical HTMS, e.g., Knudsen effusion. Depending on the detailed nature and the relative location of the potential energy surfaces in the molecular ion and in the neutral molecule and on other factors, either enhanced or reduced degrees of fragmentation accompany beam cooling. In most cases, a reduced degree of fragmentation and a reduced temperature dependence are obtained because only the vibrational ground level is occupied in adiabatically cooled neutral species [191]. Alkali halides, particularly diatomic ones, with strongly enhanced fragmentation at very low temperature are a notable exception [125,192,193]. Note that temperature-dependent ionization can become more apparent when the temperature range accessible to conventional HTMS is greatly expanded by SMBS cooling [15,125].

These effects may remain undetected in classical KMS experiments. Although only in a few instances have such temperature-dependent effects been found to be significant, they should receive more attention in future studies. The ability to readily determine relative ionization cross-sections by SMBS also allows for testing energy scaling approximations of cross-sections [18]. Such approximations depend on the similarity in shapes for σ and I^+_{jk} vs. E curves, and these are not always comparable.

6.6 High-temperature mass spectrometric determinations of ionization cross-sections

In the course of pressure or activity determinations, relative ionization cross-sections, or more often sensitivity ratios, can be measured in various ways. Some of these are:

- Comparison of ion intensities integrated against time with mass losses:
  - for known amounts of the system studied and of an inert substance, often Ag or Au, added to the former [1,4,8,13];
  - for the main species of a system studied [4,8,94,194–197]. Ionization cross-section measurements as a function of energy for different fragmentation channels were so determined for C_{60} and C_{70} [195,196].
- Comparison of intensities for species when the ratio of their pressures is fixed by congruency conditions [4,8].
- Use of consecutive (also called double or tandem) effusion cells placed in differentially heated ovens to thermally dissociate gaseous molecules produced at a lower temperature and in so doing modify the composition of the gas phase [4,8] (the low-temperature compartment is formally equivalent to an external gas reservoir).
- Use of electrochemical effusion cells to modify the composition of the gas phase at constant temperature [198–201] and to establish relations between the galvanic current, the rate of effusion, and the MS ion intensity of different constituents of the vapor [198–200].
- Use of the multiple cell method (see Section 4.2) to vaporize known amounts of different substances in a single experiment and deduce relative ionization cross-sections from mass losses [202–204].

- Successive vaporization of sequentially introduced pure metals, e.g., Ni and Ti, while the ion source is continuously operated to minimize sensitivity changes [205].
- Calculation [206,207] of relative cross-sections for atoms from activity determinations in binary alloys of known composition by the Belton–Fruehan procedure [208] and knowledge of the vapor pressures of the metals in their reference states.
- Application of the SMBS technique where the carrier gas provides an internal reference to measure relative cross-sections for constituents whose concentrations in the carrier are known. These can be:
  - gases mixed with the carrier in known amounts and
  - vapors for which gravimetric measurement of the amount of material transported and knowledge of the integrated volume of carrier gas provide the required information [15,19].
- Use of KMS cells with gas inlets [18] and beam modulation, as in SMBS, if a criterion for equilibration can be found.
- Application of laser ablation mass spectrometry to refractory materials [18,78,79], where a pulsed (typically 10–30 ns) high-power laser (~1 to 10 J/cm^2) causes quantitative local vaporization and formation of a pulsed molecular beam.

These various methods require reference substances to obtain absolute ionization cross-sections and imply that bias in ion sources, analyzers, and detectors is duly taken into account. If the reference material is not introduced into the molecular beam before collimation into the ion source, or if different beam sources are used, one should consider the possibility of geometric differences in sampling.

Ionization cross-sections of molecules, usually measured by HTMS in the course of thermodynamic studies are presented, without claim of completeness, in Tables 4 and 5. Measurements performed before ion-counting devices became widely availabe were often deduced from $\sigma\gamma$ ratios, corrected using the relation ($\gamma \sim 1/\sqrt{M}$) to estimate the mass dependence of the electron multiplier yield.

7. PRESSURE DETERMINATIONS

Absolute pressure measurements necessarily require determining the sensitivity of the mass spectrometer. This can be done in several ways and may depend on the type of instrument and on the nature of the chemical system studied [4–26]. The more common approaches are as follows.

7.1 Absolute pressure determinations

For a molecule with molar mass M and partial pressure p, the Hertz–Knudsen equation provides Δm, the mass loss by effusion after time Δt, from a Knudsen cell at temperature T, when the effective area of the orifice is aC (a is the actual area, C the Clausing coefficient discussed in Section 4.3a),

$$\Delta m = \frac{paC\sqrt{M}}{\sqrt{2\pi RT}}\Delta t \tag{35}$$

Combined with the basic mass spectrometric relation (eq. 1 in Section 2),

$$S_j = \frac{aC\sqrt{M}}{(\sum_n \Delta m_n)\sqrt{2\pi R}} \sum_n \sum_{j,k} I_{jk}\sqrt{T_n}\Delta t_n \tag{36}$$

is obtained. n here indexes the intensity data set recorded during time interval Δt_n for which a constant temperature T_n was maintained. $\Delta m = \Sigma_n \Delta m_n$ is now the cumulated mass loss. The latter often corresponds to the mass of an amount of material placed initially in the cell and caused to be completely vaporized. If necessary, correction for mass lost by the cell itself is to be made. Mass loss may also be determined by weighing the cell assembly or a pertinent part thereof before and after the experiment.

Complete vaporization of the sample may, however, be unnecessary or even impractical if its initial weight is large. Phase relations in the system should then be established prior to the experiment or be without incidence on its interpretation.

Relation 36 is applied when only one species is present or predominant in the gas phase. If an inert reference material is also studied under appropriate conditions, relative sensitivities can be determined. Where multiple temperatures are involved, eq. 36 is summed (integrated) over time intervals, Δt_n, during which the system is at a sequence of constant temperatures, T_n. Due attention should be paid to regions of temperature change and approximation or numerical integration techniques applied there. Differentiation of eq. 36 provides

$$\frac{\delta S}{S} = \left[\frac{2\delta r}{r} + \frac{\delta C}{C} + \frac{\delta(\Delta m)}{\Delta m} + \frac{\sum_n T_n^{1/2} \Delta t_n \delta I_n + 0.5(I_n \Delta t_n T_n^{-1/2} \delta T_n) + I_n T_n^{1/2} \delta(\Delta t_n)}{\sum_n I_n T_n^{1/2} \Delta t_n} \right] \tag{37}$$

where r is the radius of the orifice in the effusion cell. A reasonable evaluation of the uncertainty due to propagation of errors follows by calculating the square root of the sum of squares of the various terms in eq. 37, which yields:

$$\frac{\delta S}{S} = \left[\left(\frac{2\delta r}{r} \right)^2 + \left(\frac{\delta C}{C} \right)^2 + \left(\frac{\delta(\Delta m)}{\Delta m} \right)^2 + \frac{\sum_n (T_n^{1/2} \Delta t_n \delta I_n)^2 + 0.25(I_n \Delta t_n T_n^{-1/2} \delta T_n)^2 + [I_n T_n^{1/2} \delta(\Delta t_n)]^2}{(\sum_n I_n T_n^{1/2} \Delta t_n)^2} \right]^{1/2} \tag{38}$$

In absolute pressure determinations with the MS, an intensity corresponding to a rate of weight loss per unit time is continuously monitored (see eq. 3). The procedure is equivalent to using the instrument as a collector and determining the integrated weight loss after known time intervals. In addition, the MS provides identification of the vaporizing species and verification of the constancy of the rate of effusion at constant temperature. Especially if a single species is predominant in the vapor (≥95 %), the accuracy should be comparable to or better than that for the conventional Knudsen technique, or its variants where the effusion cell is suspended from a microbalance to determine instantaneous rates of weight loss, where target collection methods are used to monitor material transport, or where the torsion-effusion method is applied with simultaneous measurement of recoil force and of weight loss [57,58]. Inaccuracies in absolute pressures should then not exceed 10–20 % under appropriate physicochemical conditions, when inert cells are available and parasitic phenomena reduced to minimum. Otherwise, lower accuracy may result as in any weight-loss procedure. This issue is illustrated by interlaboratory comparison of the Au vapor pressure [209] by conventional as well as by MS techniques: the estimated total uncertainty for each set of experiments in a single laboratory was $\delta p/p = 55$ % and the overall weighted average error from the accepted measurements, 10 %.

Pressure calibration of the MS assembly can be performed in several other ways. These include:

- collection of a fraction of the effusate on a substrate or target diaphragm inserted in the beam collimating assembly [69,210] (for target-collection methods, see [57]);
- calculation of the rate of effusion from the galvanic current in an electrochemical Knudsen cell [198–200];

- pressure determination by conventional effusion or by torsion-effusion in experiments conducted in parallel with the MS study, but in a separate apparatus [211];
- fully simultaneous measurement of ion intensities with the MS and of effusion rates with a microbalance-mounted cell [212]; and
- adoption of pressures determined in independent investigations, or listed in tabulations of thermochemical data [32–38].

With transpiration mass spectrometry (TMS), two independent methods are available [15] for determining S_{jk}:

- From eqs. 1 and 2, it follows that

$$S_j = S_{\text{ref}}\left(\frac{\sigma_j}{\sigma_{\text{ref}}}\right)\left(\frac{d_{jk}}{d_{\text{ref}}}\right) \tag{39}$$

  S_{ref} is the independently determined sensitivity for a reference atom or molecule—typically a constituent of the transport or carrier gas. The known pressure of the latter and the observed signals provide relative sensitivities for other species in the beam. d_{jk} and d_{ref} incorporate instrumental and species-dependent factors.
- From the Ideal Gas Law, as applied in the classical transpiration approach, one derives

$$S_j = \frac{1}{R}\left(\frac{V}{n_j}\right)\frac{\sum_n(\sum_k I_{jk})\Delta t_n}{\sum_k \Delta t_n} \tag{40}$$

  where R is the gas constant, V the total volume of gas transpired containing an amount n_j of species j (SI unit mole), and Δt_n the elapsed time(s) during which ion intensities I_{jk} are measured for a given species.

Although the beam dynamics are somewhat dependent on source pressure, it is convenient to use manometric measurement of the carrier gas pressure, and to achieve each p_j determination by back-calculating a sensitivity (S_j via eqs. 1 and 2). This method is straightforward and dependable as long as the partial pressures of the sample are negligible with respect to that of the carrier gas.

When using a transport method such as transpiration mass spectrometry, similar considerations apply in the determination of absolute pressures of transported vapor species as for the Knudsen method. When relative pressures are referred to the transport (carrier) gas (e.g., Ar, N_2,…), for which the absolute pressure and ionization cross-section are generally known, one can readily convert the relative to absolute pressures if ionization cross-sections are available. Given the same care in experimental design and in measurement of the weight loss and of the total carrier flow, the error range is similar to that noted above for effusion.

7.2 Relative pressure determinations

Relative pressures are measured in mass spectrometry with two main objectives: (i) the determination of equilibrium constants in the gas phase and (ii) the determination of activities in the condensed phase.

When j species are present in the gas phase, eq. 36 can still be applied in the form,

$$\sum_n S_1 = \left(\frac{aC\sqrt{M_1}}{(\sum_n \Delta m_n)\sqrt{2\pi R}}\right)\sum_n \sum_{j,k}\left[\frac{S_1\sqrt{M_j}}{S_j\sqrt{M_1}}\left(I_{jk}\sqrt{T_n}\Delta t_n\right)\right] \tag{41}$$

where n indexes temperature intervals. As before, k indicates that more than one ion may be formed from—and monitored for—species j. Usually, the main constituent of the vapor is chosen as $j = 1$ for calibration purposes and is used as the unit to measure relative sensitivities for other species. Separate measurements or estimates of relative ionization cross-sections (and perhaps other factors discussed here, where significant) are necessary to calculate the ratios S_j/S_1.

Quantitative vaporization of a known amount of an inert (relative to the sample) and more volatile substance at the beginning of an experiment often provides a pressure calibration for the species newly studied if ionization cross-section ratios are known or estimated. Prior knowledge of the vapor pressure of the added substance is not a prerequisite in the procedure, but an advantage. Samples of a few mg of Ag or Au in the form of a thin foil are commonly used for this purpose. The vapor pressures of these elements are known and mass spectrometrically measurable at their melting points. Observation of a plateau in the rate of vaporization at the melting point hence provides a calibration of the temperature scale as well as of the pressure. Dual calibration by this procedure and by quantitative vaporization of the aliquots allows one to check mass spectrometer sensitivity changes during a set of experiments and to detect abnormal working conditions or parasitic phenomena.

Equations 1 and 41, or equivalent forms, can also be used in conjunction with other relations that provide absolute pressures, e.g., the flux of effusing molecules calculated from the galvanic current in an electrochemical effusion cell [198–200], a known equilibrium between two or more gaseous species, e.g., $X_2(g) = 2\,X(g)$, a relation between rates of effusion such as when vaporization is congruent or another restriction imposed by the phase rule. When a series of experiments is performed with the same settings of the ion source and regular intermediate verification is made with a pure substance, it is possible to use the sensitivity, thus determined for a major species, in consecutive experiments where this atom or molecule has become of minor importance in the vapor [213].

Determination of absolute pressures is not necessary in order to study equimolecular exchange reactions of the type $A(s) + A(g) = A_2(g)$ or $AB(g) + C(g) = AC(g) + B(g)$. Calculation of their equilibrium constants indeed only requires knowing or estimating relative ionization cross-sections or sensitivities.

For thermodynamic studies of condensed solid or liquid phases in multicomponent systems, the partial pressure p_j of a monomeric species associated with component j is to be related to the corresponding pressure p_j^{rs} in equilibrium with the pure component in its reference state at the same temperature, or with an auxiliary reference state with pressure p_j^{as} and activity $a_j^{\mathrm{as}} = p_j^{\mathrm{as}}/p_j^{\mathrm{rs}}$. The activity of component j in the system is then defined by the relation

$$a_j = \frac{p_j}{p_j^{\mathrm{rs}}} = \frac{a_j^{\mathrm{as}} p_j}{p_j^{\mathrm{as}}} \tag{42}$$

The relative activity a_j is related to the corresponding chemical potential (partial molar Gibbs energy) by:

$$\mu_j = \mu_j^{\ominus} + RT \ln a_j \tag{43}$$

where $\mu^{\ominus}$ is the standard chemical potential.

These determinations require very accurate measurement of partial pressures

- because enthalpies or Gibbs energies of mixing are generally at least 10 times lower than enthalpies or Gibbs energies of vaporization and
- because the final result is the difference of two measured large quantities, each with their own uncertainties.

For these reasons, an important potential source of error in studies of alloys by conventional high-temperature mass spectrometry is the reproducibility of all instrumental parameters between different experiments, mainly because

- the ion source ordinarily has to be switched off and exposed to air and
- the Knudsen effusion assembly needs to be dismantled to introduce a new sample or cell, with consequent minor but often critical changes in system geometry.

A number of approaches avoid these inconveniencies. The most direct one involves use of twin or multiple Knudsen cells [214–216], in which one cell contains a pure constituent and the other(s) a compound or an alloy. The cells are, in general, sequentially positioned mechanically in relation to the MS. Stationary twin effusion cells located inside a common third compartment [217] imply study of distinct elements or of isotopes of the same element.

The ion intensity ratio for a given gaseous atom as measured successively from two or more cells is directly related to the activity by:

$$a_j = (I_j T/S_j)_{\text{alloy}}/(I_j T/S_j)_{\text{ref}} \tag{44}$$

which may be simplified to

$$a_j = (I_j)_{\text{alloy}}/(I_j)_{\text{ref}} \tag{45}$$

if temperature and sensitivity are the same for the two cells. In practice, it may be difficult to meet these conditions [218] for reasons mentioned above. Use of restrictive collimation [74] to ensure that the MS is viewing directly inside the effusion orifices increases the quality of the measurements by eliminating parasitic re-evaporated or scattered molecular contributions and parallax discrimination in the ionization chamber. This arrangement has several additional advantages:

- It allows studying multicomponent alloys or solutions with a multiple cell oven having at least one cell for the solution and a cell for the reference state of each component.
- It is less sensitive to absolute temperature measurements [218] than single cell arrangements.
- The number of data points obtainable in one or a few experiments is larger than in any other MS procedure [219].
- Pressure ratios for the same species are much less dependent on the characteristics of the ionization source.
- Causes of inaccuracy can be reduced to reading uncertainties, since instrumental and physical factors cancel out in the determination of activities.
- The cells with the reference states provide a permanent reference sensitivity for each volatile component. If necessary, secondary reference states—e.g., intermediate, preferably univariant, compositions—can be used to optimize the procedure and the quality of the results [220].

Two critical requirements are:

- The steady state temperature difference between all cells should be less than ~0.1 K. Contrary to prevailing opinion, this condition is generally easier to achieve above 1000 °C than at lower temperatures [216].
- There should be no transfer of gaseous species from the furnace, shields or adjacent cells into cells where activities—i.e., partial pressures—are very different.

Uniformity of temperature among cells can be checked by loading each of these with aliquots identical in volume, mass, chemical composition, proportion of phases present, and by measuring ion intensity ratios as a function of temperature [204,216]. The impact of transfer of material by reverse-effusion cannot be predicted, but anomalous results in activity vs. composition can be detected [221] and new reference compositions selected. Gibbs–Duhem integration can in addition be used—if activities

of all components are directly measurable—to check either the internal consistency of simultaneous determinations, or equilibrium in the cells [50,221,222].

A second approach to relative pressure determinations involves operating the MS system—ion source, analyzer, detector(s)—in a continuous fashion, by introducing a vacuum valve between the compartment with the Knudsen cell assembly and the ion source housing [205,223,224]. Small relative variations in sensitivity have been achieved during studies of amalgams (<3 % [223]) and of Ni–Al–Ti alloys (0.5 to 17 % [205]). If sensitivity is constant with time, such arrangements are particularly suitable for activity measurements when experiments with the pure metals as reference are performed in between measurements with alloys. Advantages of the method are:

- The stability of the instrument can be extremely high because of the special procedure followed to change samples, as has been shown over a period of 30 days [205].
- There is little difficulty in determining very low thermodynamic activities by comparing, in successive runs, ion intensities for a component of the alloy and for the corresponding pure metal.
- Single cells can be small, which facilitates rendering their temperature homogeneous.
- Loading another sample in the Knudsen cell is not time-consuming (as little as 1 h for a complete vent-reload-pumpdown cycle).
- The extremely low background ion intensities achievable allow measurement of partial pressures $\leq 10^{-7}$ Pa [225], and even 10^{-8} Pa in Knudsen cells [226].
- The ion source of the mass spectrometer can remain extremely clean and may require perhaps only one opening per year of use.

The most critical parameter in the uncertainty associated with the procedure is measurement of the absolute temperature of the cells. Next, and to a lesser degree, is reproducibility in positioning the cells.

The reproducibility of the two methods described above for activity determinations can be within 5 to 10 %.

A third method, frequently utilized for binary alloys [14,24] was introduced by Belton and Fruehan [208,227]. It involves use of the Gibbs–Duhem relation and measurement of ion intensity ratios for the different components in samples of known composition. The procedure relies on:

- simultaneous measurement of two pertinent ion intensities for binary alloys (three for ternary, etc.), for a wide range of compositions up to one where the activity is known;
- constancy of the sensitivity ratios during successive experiments;
- extrapolation instead of measurement for the pure metals; and
- knowledge of the vapor pressure of the pure metals in their reference states (if required).

The advantage of this method is that it can be easily applied in conventional KMS assemblies. A disadvantage is that the Gibbs–Duhem relation can no longer be used to perform an independent cross-check on the variation of the activity data with concentration, and that there is no criterion to detect systematic errors. For these or other reasons, study of alternate alloys may yield ratios of ionization cross-sections for the same two elements that differ by 10 to 25 % [206,207]. Statistical analysis, nevertheless, remains possible for the individual data points measured in each experiment as a function of temperature, for a set of experiments as a function of concentration, and finally for the thermochemical parameters determined for the solution under study [228,229]. The Belton–Fruehan method has been combined with phase-sensitive detection and extended to activity determinations in the system $FeO–MgO–SiO_2$ [230].

8. THERMODYNAMIC CALCULATIONS

8.1 Second and Third Law calculations

Calculation of thermochemical data by application of the Second Law of Thermodynamics [34,37,38,231–235] is based on the equation:

$$\Delta_r H^{\ominus}(T) = -R \frac{\mathrm{d} \ln K_p(T)}{\mathrm{d}(1/T)} \tag{46}$$

to determine the enthalpy difference $\Delta_r H^{\ominus}(T)$ associated with reaction r at the median temperature T.

This application presumes that $\Delta_r H^{\ominus}(T)$ is (nearly) constant in a given temperature interval and that the equilibrium constant $K_p(T)$ was measured a sufficient number of times over that interval. The entropy difference $\Delta_r S^{\ominus}(T)$ may then be calculated from the relation

$$\Delta_r G^{\ominus}(T) = -\mathrm{RT}\ln K_p = \Delta_r H^{\ominus}(T) - T\Delta_r S^{\ominus}(T) \tag{47}$$

The resulting average $\Delta_r H^{\ominus}(T)$ and $\Delta_r S^{\ominus}(T)$ values can be reduced to a conventional reference temperature, Θ = 298.15 or 0 K. $\Delta_r H^{\ominus}(\Theta)$ can be directly computed with the "sigma plotting" procedure that takes into account the variation in $\Delta_r H^{\ominus}(T)$ with temperature [234].

In Third Law calculations, eq. 47 is also used, but with an independently known value of $\Delta_r S^{\ominus}(T)$. The latter can be calculated with conventional Third Law entropies $S^{\ominus}_j$ based on measured or theoretically calculated heat capacities of condensed phases and gases. The convention is that the entropy of fully equilibrated substances is zero at 0 K.

In many cases, in order to directly reduce data to the reference temperature Θ, eq. 47 is replaced by eq. 48:

$$\Delta_r G^{\ominus}(T) = -\mathrm{RT}\ln K_p(T) = \Delta_r H^{\ominus}(\Theta) - T\Delta_r\{[G^{\ominus}(T) - H^{\ominus}(\Theta)]/T\} \tag{48}$$

In eq. 48, $[G^{\ominus}(T) - H^{\ominus}(\Theta)]/T$ is the free energy function (sometimes labeled as fef or Φ), a thermodynamic function closely related to the entropy. As above, normally Θ = 0 or 298.15 K, depending on the tabulation.

Fundamentally, data treatment with the Second and Third Laws of Thermodynamics is equivalent, but the resulting error estimates may be quite different.

8.2 Thermal functions

Thermodynamic functions $\{C^{\ominus}_p, S^{\ominus}(T), [H^{\ominus}(T) - H^{\ominus}(\Theta)]$ and $[G^{\ominus}(T) - H^{\ominus}(\Theta)/T]\}$ of condensed phases are mostly based on experimental determination of heat capacities as a function of temperature down to low temperatures. For gaseous molecules, the corresponding functions are generally calculated with statistical mechanical formulae [34,37,38,236–238] from molecular parameters, i.e., geometry (interatomic distances, bond angles), vibrational frequencies, excitation energies, and multiplicities of electronic states [237,239], which are primarily deduced from infrared, Raman, or ultraviolet spectroscopic studies of gaseous or matrix-isolated species. In the last few decades, molecular data have been obtained increasingly from quantum-chemical calculations [240–244]. Structural data may also be derived from electron diffraction measurements in the gas phase.

In the absence of experimental or calculated data, satisfactory estimates can usually be made by a variety of procedures [245]. For molecules, molecular constants can often be estimated by analogy with those of closely related known species. Trends along rows and columns in the periodic table of elements assist in selecting the more probable molecular parameters and geometry. Simple rules [246–248] help in estimating interatomic distances and vibrational frequencies for which approximate values can also be calculated with the central force or the valence force [237] approximations. Detailed models have been developed for large molecules [249] to obtain complete sets of vibrational

frequencies. For complex molecules, a dimensional model [250–252] affords calculation of the non-electronic part of the entropy by analogy with molecules of the same stoichiometry. The accuracy of this empirical approach depends on the number of molecules available for comparison. Entropies and related functions have also been estimated by interpolation of the values for known homologous molecules and adjustment for differences in symmetry numbers [253].

Uncertainties in thermodynamic functions calculated from experimental molecular parameters are small, i.e., ~ ±0.2 to 0.4 J K^{-1} mol^{-1}. When estimates are based on models and comparisons with known molecules, uncertainties of ±0.5 to 1 J K^{-1} mol^{-1} per bond may obtain in the absence of low vibrational frequency modes (≤150 cm^{-1}) and low-lying electronic states ($\varepsilon_i \leq 10\,000$ cm^{-1}).

The standard pressure was 1 atm = 1.013 25 MPa until 1979, after which date it became 1 bar = 0.1 MPa [254,255]. It can be verified that standard entropies and free energy functions are increased by R ln(1.013 25) when converting such data from the previous to the present reference state. The dimensionless quantities p_i/atm used in calculating equilibrium constants are also changed, partial pressures reported in atm being multiplied by the factor 1.013 25 in order to obtain the corresponding values expressed in bar: p_i/bar = 1.013 25 p_i/atm. Reaction enthalpies and dissociation energies are, hence, not changed by the modification in the standard reference pressure. Sublimation, boiling, and decomposition temperatures remain defined as being those temperatures where the total pressure reaches 1 atm.

8.3 Accuracy and precision in Second and Third Law calculations

In discussing accuracy and precision, distinction is to be made between random and systematic uncertainties and errors, as in any other experimental technique.

Random errors in the primary measurements entail statistical scatter among individual data points and result in a corresponding uncertainty in $\Delta_r H^\ominus(T)$ and $\Delta_r H^\ominus(\Theta)$, whether calculated by the Second or by the Third Law methods. Systematic errors and their nature, on the contrary, have a different incidence in the two types of data treatment, despite their fundamental equivalence.

In Second Law analysis, the incidence of random errors is minimized by least-squares fitting methods. The error magnitude is characterized by the standard deviation of the fit, S_{fit}, and the derived standard deviations for the coefficients of the regression line. The standard deviation is, hence, known for the thermodynamic quantities $\Delta_r H^\ominus$ and $\Delta_r S^\ominus$ derived from equilibrium constants measured in some temperature interval. Statistical formulae for computing the standard deviations by use of the curvature matrix are presented in "Analysis of Interlaboratory Measurements on the Vapor Pressure of Gold" [209]. They are reproduced here to illustrate the treatment that provides error estimates in the Second Law analysis of the Clausius–Clapeyron equation, in the form ln $K_p = A + BX$ with $X = 1/T$, $A = \Delta_r S^\ominus/RT$, and $B = -\Delta_r H^\ominus/R$, viz.:

$$S_A = \left[\frac{1}{N} + \frac{\bar{X}^2}{\sum_k (X_k - \bar{X}^2)} \right]^{1/2} S_{\text{fit}} \tag{49}$$

$$S_A = \left[1 / \sum_k \left(X_k - \bar{X}^2 \right) \right]^{1/2} S_{\text{fit}} \tag{50}$$

To allow intercomparison of distinct measurements, Second Law results should be published with the standard error of estimate for the fit, S_{fit}, as well as S_A and S_B for the coefficients A and B.

For Third Law results, the standard deviation of the data set or lot [i.e., for the average of N values of $\Delta_r H^\ominus(\Theta)$] and the standard deviation of the mean should be reported. It should be clearly stated which of these alternative standard deviations is used to estimate uncertainties, and the number of data

points in the lot should be given. If not already introduced by the investigator, Student's t-coefficient can then provide a confidence interval (typically, the 90 or 95 % confidence level). It should be checked that the individual data vary randomly as a function of temperature. In general, the process that obtains replicate values of $\Delta_f H^{\ominus}(\Theta)$ is not an averaging process. The simple standard deviation from the average is, hence, more appropriate because the standard deviation of the mean applies only when averaging means from replicate data lots.

Both public domain and commercial software programs now greatly facilitate descriptive statistical analysis of individual experiments and analysis of variance (ANOVA) between successive or independent series of measurements. Users should be aware that all software packages do not define statistical quantities in the same way and that the robustness of algorithms may greatly vary.

Systematic errors, after exclusion of easily detected instabilities, include (i) nearly constant, (ii) gradually changing differences between the "true" and the measured (or calculated) values of independent variables: (a) temperature, (b) three interrelated quantities, (b_1) intensities, (b_2) ionization cross-sections, (b_3) derived pressures, and (c) thermal functions. The effects of these systematic errors on Second and Third Law results can be quite different.

In Third Law calculations, systematic errors generally cause the final result to vary systematically with temperature. The resulting "trend" can be detected by displaying the individual reaction enthalpies of the lot as a function of measured temperatures [34,38]. In Second Law calculations, systematic errors may not be easy to find because they often vary with the same or nearly the same functionality as the processes under investigation [256].

Agreement between Second and Third Law results, and the absence of trends in the latter, are usually good indicators that causes of systematic errors are under control. Fortuitous compensations, nevertheless, remain possible. Concordance between Second and Third Law results is a necessary but insufficient condition for absence of systematic errors [257]. Development of this theme [258] and of the outline of a thermodynamic theory of errors [259,260] is beyond the scope of the present report.

The above discussion implies that Second and Third Law results, after careful examination and evaluation of their associated uncertainties, should be compatible. The Third Law result should be located within the uncertainty interval of the Second Law result. If the two are incompatible, many authors prefer to accept the Third Law result if the required thermal functions are sufficiently well established. That result is indeed normally less sensitive to random error in measurements and affords easier identification of trends due to systematic errors. Entropies and free energy functions should, however, be independently calculated rather than adjusted to cause agreement between the two treatments.

With respect to "Presentation in the primary literature of numerical data derived from experiment" [261] and "Assignment and presentation of uncertainties of the numerical results of thermodynamic measurements" [262–264], the following remarks seem appropriate.

In thermochemical studies by mass spectrometry at high temperatures, it has been customary to assign either estimated uncertainty limits only or to combine the latter with statistically calculated standard deviations. In many instances, the latter have actually not been standard deviations of the mean [265] but standard deviations of the data set. These standard deviations were, furthermore, often doubled, corresponding to a high (~90 %) confidence level and even wider error estimate. The incidence of assumptions made in processing the data and uncertainties or defects in the physical models used [258] have in general been duly taken into account. To this effect, propagation of errors was considered and based on differentiation of the relations used in the investigation and insertion of appropriate uncertainties. For completeness, it is added that in general the square root of the sum of squares of the different terms was used, considering that it is unlikely that all terms would affect the result in the same direction. These procedures explain why mass spectrometric results occasionally seem rather uncertain in comparison with other thermochemical data reported with uncertainty limits corresponding solely to the standard deviation of the mean.

Examination of the results obtained for a given system in distinct laboratories or in the same one at different times shows reproducibility and repeatability to be comparable in the method discussed and

in other experimental procedures for the determination of pressures of single species and of thermochemical data based thereon.

As stressed before, the mass spectrometric method allows determination of absolute or relative pressures for all observable species that are in equilibrium among themselves and with the condensed phase(s) present in the system, including the container. The amount of information gained may, therefore, be larger than strictly needed for a complete evaluation of the results and render the system overdetermined.

9. SUMMARY AND RECOMMENDATIONS

The basic principles and sources of uncertainty in high-temperature mass spectrometry have been considered here. Particular attention has been paid to

- the fidelity of gas/vapor sample extraction for MS analysis;
- the electron impact process and mass spectral analysis of representative gas/vapor samples;
- the conversion of primary ion intensity data into partial pressures, for which absolute or relative ionization cross-sections are required; and
- the calculation and selection of thermal functions and parameters associated with the conversion of pressures into thermodynamic quantities.

In considering the present status of HTMS methods in general, and the incidence of ionization cross-sections in particular, the following points are noteworthy. Since an earlier review on the subject of ionization cross-sections in HTMS [13], additional attention has been given to improving the experimental database and the theoretical calculation of (high-temperature) ionization cross-sections.

The present study has examined the nature and extent of uncertainties and experimental inaccuracies inherent to the HTMS method and noted areas where further work is desirable. The results, for the most part, were found to be in good to excellent agreement with those of other physical and chemical methods, where such comparisons were possible. In many instances, absolute or relative pressure data resulted from comparative measurements or from experiments based on weight-loss measurements. For the major atoms and molecules present in the gas phase, the effect of uncertain knowledge in ionization cross-sections can be markedly attenuated or removed with careful work and/or special techniques. As a consequence, it is no longer commonly the case that "vapor pressures are not infrequently reported which disagree by a factor of 100 or more" [266]. The hope expressed when HTMS was initiated (viz. to see inconsistencies in pressures decrease to a factor of perhaps two or better) can usually be realized, even for minor constituents of the vapor.

Significant progress has been made in the development of systematically calculated and critically evaluated databases of ionization cross-sections for the elements [135–139,141–143]. For molecules, theoretical and semi-theoretical models have been developed for calculating ionization cross-sections [181–185,187]. Progress in the measurement of molecular cross-sections [146–149] is encouraging, although incomplete. Empirical corrections [20,175] to the simple additivity rule of atomic cross-sections have been deduced, a development that markedly increases the validity of estimated molecular ionization cross-sections. Irregularities and deviations from generalizations based on the limited information available may, nevertheless, be anticipated. This conjecture may justify additional experimental and theoretical investigation of ionization cross-sections, of the parameters that govern direct vs. dissociative ionization, and of their dependence on the electronic structure of the atoms forming the molecule. Temperature dependence of molecular ionization cross-sections, that was expected [5] on general grounds, has been observed for a few molecules [18,20] and deserves to be studied in a larger number of instances.

In conclusion, it may be stressed that, despite limitations mentioned here for HTMS and the frequent need to estimate ionization cross-sections in order to quantify MS data, the method has and should continue to provide valuable information, not otherwise obtainable, on the thermochemical be-

havior of materials and processes at high temperatures and otherwise extreme environments. The hope is expressed that investigators applying the methodology analyzed here will measure absolute or relative ionization cross-sections whenever possible and that investigators intending to generate atomic or molecular beams in order to carry out physical measurements will find useful information in the present report and discussion of known interferences in cells used to generate such beams by effusion or high-pressure techniques.

ACKNOWLEDGMENTS

We would like to thank Dr J. B. Mann for kindly making available the detailed computer outputs for his calculations of $\sigma(E)$ that were used in developing the fits for program SIGMA.

ABBREVIATIONS

HTMS	high-temperature mass spectrometry
KMS	Knudsen effusion mass spectrometry
LVMS	laser vaporization mass spectrometry
MS	mass spectrometer/mass spectrometry
SMBS	supersonic molecular beam sampling
SSMS	spark source mass spectrometry
TMS	transpiration mass spectrometry
UHV	ultrahigh vacuum

REFERENCES

1. W. A. Chupka and M. G. Inghram. *J. Chem. Phys.* **21**, 371–372 (1953); *J. Phys. Chem.* **59**, 100 (1955).
2. R. E. Honig. *J. Chem. Phys.* **22**, 126 (1954).
3. R. F. Porter. In *High Temperature: A Tool for the Future*, pp. 182–186, Stanford Research Institute, Menlo Park, CA (1956).
4. M. G. Inghram and J. Drowart. In *High Temperature Technology*, pp. 219–240, McGraw-Hill, New York (1959).
5. J. Drowart. In *Condensation and Evaporation of Solids*, E. Rutner, P. Goldfinger, J. P. Hirth (Eds.), pp. 255–310, Gordon and Breach, New York (1964).
6. P. Goldfinger. In *Mass Spectrometry*, R. I. Reed (Ed.), pp. 265–281, Academic Press, London (1965).
7. J. Drowart and P. Goldfinger. *Adv. Mass Spectrom.* **3**, W. L. Mead (Ed.), pp. 923–943, The Institute of Petroleum, London (1966).
8. J. Drowart and P. Goldfinger. *Angew. Chem., Int. Ed.* **6**, 581–596 (1967).
9. R. T. Grimley. In *The Characterization of High-Temperature Vapors*, J. L. Margrave (Ed.), pp. 195–243, Wiley, New York (1967).
10. J. W. Hastie and J. L. Margrave. *High Temp. Sci.* **1**, 481–495 (1969).
11. J. Drowart. In *Mass Spectrometry*, J. Marsel (Ed.), pp. 187–242, "J. Stefan" Institute, Ljubljana, Yugoslavia (1971).
12. L. N. Gorokhov and G. A. Semenov. *Adv. Mass Spectrom.* **5**, A. Quayle (Ed.), pp. 349–358, The Institute of Petroleum, London (1971).
13. F. E. Stafford. *High Temp. High Press.* **3**, 213–224 (1971).
14. C. Chatillon, J. Drowart, A. Pattoret. *High Temp. High Press.* **7**, 119–148 (1975).
15. D. W. Bonnell and J. W. Hastie. In *Characterization of High Temperature Vapors and Gases NBS SP-561/1*, J. W. Hastie (Ed.), pp. 357–409, NIST, Gaithersburg, MD (1979).

16. C. Chatillon, M. Allibert, A. Pattoret. In *Characterization of High Temperature Vapors and Gases NBS SP-561/1*, J. W. Hastie (Ed.), pp. 181–210, NIST, Gaithersburg, MD (1979).
17. K. A. Gingerich. In *Molecular Species in High Temperature Vaporization. Current Topics in Material Science*, E. Kaldis (Ed.), Chap. 5, pp. 345–462, North-Holland, Amsterdam (1980).
18. J. W. Hastie. *Pure Appl. Chem.* **56**, 1583–1600 (1984).
19. J. W. Hastie and D. W. Bonnell. In *Thermochemistry and its Applications to Chemical and Biochemical Systems*, M. A. V. Ribeiro da Silva (Ed.), pp. 183–233, Reidel Publishing, Boston (1984).
20. J. Drowart. In *Adv. Mass Spectrom.*, J. F. J. Todd (Ed.), pp. 195–214, John Wiley, New York (1986).
21. L. N. Sidorov, L. V. Zhuravleva, I. D. Sorokin. *Mass Spectrom. Rev.* **5**, 73–97 (1986).
22. E. R. Plante and J. W. Hastie. In *Specialist Periodical Reports: Mass Spectrometry* **10**, pp. 357–378, Royal Soc., London (1989).
23. J. W. Hastie and J. P. Hager. In *Proc. The Elliot Symposium on Chemical Process Metallurgy*, pp. 263–286, Iron and Steel Soc., Warrendale, PA (1990).
24. K. Hilpert. In *Structure and Bonding*, pp. 97–198, Springer Verlag, Berlin (1990).
25. K. Hilpert. *Rapid Commun. Mass Spectrom.* **5**, 175–187 (1991).
26. E. Kato. *J. Mass Spectrom. Soc. Jpn.* **41**, 297–316 (1993).
27. V. L. Stolyarova and G. A. Semenov. *Mass Spectrometric Study of the Vaporization of Oxide Systems*, J. H. Beynon FRS (Ed.), John Wiley, New York (1994).
28. L. N. Sidorov. *Int. J. Mass Spectrom. Ion Processes* **118/119**, 739–754 (1992).
29. A. G. Gaydon. *Dissociation Energies and Spectra of Diatomic Molecules*, Chapman and Hall, London (1968).
30. L. V. Gurvich, G. V. Karatsevtchev, V. N. Kondratiev, Y. A. Lebedev, V. A. Medvedev, V. K. Potapov, Y. S. Khodeev. *Energii Razryva Khimicheskikh Svyazei*, Izdatlstvo Nauka, Moscow (1974).
31. K. P. Huber and G. Herzberg. *Molecular Spectra and Molecular Structure IV. Constants of Diatomic Molecules*, Van Nostrand Reinhold, New York (1979).
32. R. Hultgren, P. D. Desai, D. T. Hawkins, M. Gleiser, K. K. Kelley, D. Wagman. *Selected Values of the Thermodynamic Properties of the Elements*, American Society of Metals, Metals Park, OH (1973).
33. K. C. Mills. *Thermodynamic Data for Inorganic Sulphides, Selenides and Tellurides*, Butterworths, London (1974).
34. M. W. Chase, Jr., C. A. Davies, J. R. Downey, Jr., D. J. Frurip, R. A. McDonald, A. N. Syverud. *JANAF Thermochemical Tables*, 3rd ed. (*J. Phys. Chem. Ref. Data* **14**, Suppl. No. 1), American Chemical Society, Washington, DC (1985).
35. O. Knacke, O. Kubaschewski, K. Hesselmann. *Thermochemical Properties of Inorganic Substances*, 2nd ed., Springer Verlag, Berlin (1991).
36. I. Barin. *Thermochemical Data of Pure Substances*, 4th ed., VCH, Weinsheim (1993).
37. L. V. Gurvich, I. V. Veyts, C. B. Alcock. *Thermodynamic Properties of Individual Substances*, 4th ed., Vols. 1–3, Hemisphere Publishing, New York (1989).
38. M. Chase, Jr. *NIST-JANAF Thermochemical Tables*, 4th ed., *J. Phys. Chem. Ref. Data Monograph 9*, National Institute of Standards and Technology, Gaithersburg, MD (1998).
39. J. L. Franklin, J. G. Dillard, H. M. Rosenstock, J. T. Herron, K. Draxl, F. H. Field. *Ionization Potentials, Appearance Potentials and Heats of Formation of Gaseous Positive Ions.* **NSRDS-NBS 26**, National Technical Information Service, Washington, DC (1969).
40. S. G. Lias, J. E. Bartness, J. F. Liebman, J. L. Holmes, R. D. Levin, W. G. Mallard. *J. Phys. Chem. Ref. Data* **17**, Suppl. 1 (1988).
41. "Isotopic Compositions of the Elements 1997", *Pure Appl. Chem.* **70**, 217–235 (1998).

42. "Atomic Weights of the Elements", *Pure Appl. Chem.* **68**, 2349–2384 (1980); *ibid.* **68**, 2339–2359 (1996).
43. C. S. Williams. *Appl. Opt.* **51**, 564–571 (1961).
44. The function of shutters is comparable here and in optical instruments. The functions of shutters and of shut-off valves are entirely different.
45. M. L. McGlashan. *J. Chem. Thermodyn.* **22**, 653–663 (1990).
46. E. K. Storms and B. A. Mueller. In *Characterization of High Temperature Vapors and Gases* **NBS SP-561/1**, J. W. Hastie (Ed.), pp. 143–152, Gaithersburg, MD (1979).
47. E. K. Storms. *High Temp. Sci.* **1**, 456–465 (1969).
48. C. Chatillon, M. Allibert, R. Moracchioli, A. Pattoret. *J. Appl. Phys.* **47**, 1690–1693 (1976).
49. M. Tmar and C. Chatillon. *J. Cryst. Growth* **89**, 501–510 (1988).
50. L. Martin-Garin, C. Chatillon, M. Allibert. *J. Less-Common Met.* **63**, 9–23 (1979).
51. P. Clausing. *J. Vac. Sci. Technol.* **8**, 636–646 (1971), translation of *Ann. Physik* **12**, 961 (1932).
52. W. C. DeMarcus and E. H. Hopper. *J. Chem. Phys.* **23**, 1344 (1955).
53. A. S. Berman. *J. Appl. Phys.* **36**, 3356 (1965).
54. R. D. Freeman and J. G. Edwards. In *The Characterization of High Temperature Vapors*, J. L. Margrave (Ed.), pp. 508–529, John Wiley, New York (1968).
55. J. W. Ward and M. V. Fraser. *J. Chem. Phys.* **50**, 1877–1882 (1969).
56. R. J. Cole. *Prog. Astron. Aeronaut.* **51**, 261–272 (1976).
57. D. Cater. In *Characterization of High Temperature Vapors and Gases*. *NBS SP-561/1*, J. W. Hastie (Ed.), pp. 3–38, NIST, Gaithersburg, MD (1979).
58. P. G. Wahlbeck. *High Temp. Sci.* **21**, 189–232 (1986).
59. C. I. Whitman. *J. Chem. Phys.* **20**, 161–164 (1952).
60. K. Motzfeldt. *J. Phys. Chem.* **59** , 139–147 (1955).
61. G. M. Rosenblatt. In *Evaporation from Solids, Treatise of Solid State Chemistry, Vol. VI, Surfaces*, N. B. Hannay (Ed.), pp. 165–239, Plenum Press, New York (1976).
62. J. W. Ward and M. V. Fraser. *J. Chem. Phys.* **49**, 3743–3750 (1968).
63. G. M. Rosenblatt. *J. Electrochem. Soc.* **110**, 563–569 (1963).
64. C. Chatillon, P. Rocabois, C. Bernard. *High Temp. High Press.* **31**, 413–432 (1999).
65. A. Vander Auwera-Mahieu and J. Drowart. *Chem. Phys. Lett.* **1**, 311–313 (1967).
66. C. A. Stearns, F. J. Kohl, G. C. Fryburg, R. A. Miller. In *Characterization of High Temperature Vapors and Gases*. *NBS SP-561/1*, J. W. Hastie (Ed.), pp. 303–355, NIST, Gaithersburg, MD (1979).
67. C. A. Stearns, F. J. Kohl, G. C. Fryburg, R. A. Miller. NASA Technical Memorandum, 73720, pp. 1–55 (1977).
68. U. Merten and W. E. Bell. In *The Characterization of High-Temperature Vapors*, J. L. Margrave (Ed.), pp. 91–114, John Wiley, New York (1967).
69. A. Pattoret, J. Drowart, S. Smoes. *Bull. Soc. Franç. Ceram.* **77**, 75–90 (1967).
70. J. Drowart, A. Pattoret, S. Smoes. *Proc. Brit. Ceram. Soc.* **8**, 67–89 (1967).
71. C. Chatillon, M. Allibert, A. Pattoret. *High Temp. Sci.* **8**, 233–255 (1976).
72. C. T. Foxon, B. A. Joyce, R. F. C. Farrow, R. M. Griffiths. *J. Phys. D (Appl. Phys.)* **7**, 2422–2435 (1974).
73. J. W. Hastie, D. W. Bonnell, E. R. Plante. *High Temp. Sci.* **13**, 257–277 (1980).
74. P. Morland, C. Chatillon, Ph. Rocabois. *High Temp. Mat. Sci.* **37**, 1–21 (1997).
75. J. W. Hastie. *Int. J. Mass Spectrom. Ion Phys.* **16**, 89–100 (1974).
76. A. Kaldor and J. W. Hastie. *Chem. Phys. Lett.* **16**, 328–331 (1972).
77. H. Bloom and J. W. Hastie. *J. Chem. Phys.* **49**, 2230–2236 (1968).
78. L. N. Sidorov, A. Ya. Borshchevskii, O. V. Boltaliva, I. D. Sorokin, E. V. Skokan. *Int. J. Mass Spectrom. Ion Processes* **73**, 1–11 (1986).
79. J. W. Hastie. *Chem. Phys. Lett.* **17**, 195–198 (1972).

80. T. P. J. H. Babeliowsky. *Physica* **28**, 1150–1154 (1962); *J. Chem. Phys.* **38**, 2036–2037 (1963).
81. S. Banon, C. Chatillon, M. Allibert. *High Temp. Sci.* **15**, 129–149 (1982).
82. C. Brunné. *Int. J. Mass Spectrom. Ion Processes* **76**, 125–237 (1987).
83. M. G. Inghram, R. J. Hayden, D. C. Hess. In *Mass Spectroscopy in Physics Research, NBS Circular 522*, pp. 257–264, National Bureau of Standards (now The National Institute of Standards and Technology), NIST, Gaithersburg, MD (1953).
84. R. C. Lao, R. Sander, R. F. Pottie. *Int. J. Mass Spectrom. Ion Phys.* **10**, 309–313 (1972–73).
85. R. F. Pottie, D. L. Cocke, K. A. Gingerich. *Int. J. Mass Spectrom. Ion Phys.* **11**, 41–48 (1973).
86. M. Van Gorkom and R. E. Glick. *Int. J. Mass Spectrom. Ion Phys.* **4**, 203–218 (1970).
87. H. E. Stanton, W. A. Chupka, M. G. Inghram. *Rev. Sci. Instrum.* **27**, 109 (1956).
88. M. G. Inghram, cited in [6].
89. F. A. White. *Mass Spectrometry in Science and Technology*, John Wiley, New York (1968).
90. G. Mathieu and L. Lamberts. *Int. J. Mass Spectrom. Ion Phys.* **31**, 125–133 (1979).
91. M. Van Gorkom, D. P. Beggs, R. E. Glick. *Int. J. Mass Spectrom. Ion Phys.* **4**, 441–450 (1970).
92. M. Yamawaki, M. Yasumoto, C. Nakano, M. Kanno. *High Temp. High Press.* **14**, 423–430 (1982).
93. J. W. Hastie, D. W. Bonnell, P. K. Schenck. *High Temp. Sci.* **25**, 117–142 (1988); *Pure Appl. Chem*. **72**, 2111–2126 (2000).
94. S. Smoes, J. Drowart, J. M. Weltner. *J. Chem. Thermodyn.* **9**, 275–292 (1977).
95. R. T. Grimley and J. A. Forsman. In *Characterization of High Temperature Vapors and Gases*. *NBS SP-561/1*, J. W. Hastie (Ed.), pp. 211–230, NIST, Gaithersburg, MD (1979).
96. J. W. Ward, R. L. Bivins, M. V. Fraser. *J. Vac. Sci. Technol*. **7**, 206–210 (1970).
97. N. A. Gokcen. *J. Phys. Chem.* **69**, 3538–3541 (1965).
98. H. S. W. Massey and E. H. S Burhop. *Electronic and Ionic Impact Phenomena*, Clarendon Press, Oxford (1952).
99. H. S. W. Massey, E. H. S Burhop, H. B. Gilbody. *Electronic and Ionic Impact Phenomena,* 2nd ed., Vols. I–IV, Clarendon Press, Oxford (1969).
100. S. M. Mott and H. S. W. Massey. *The Theory of Atomic Collisions*, Clarendon Press, Oxford (1970).
101. U. Fano and L. Fano. *Physics of Atoms and Molecules*, University of Chicago Press, Chicago (1972).
102. J. Berkowitz. *Photoabsorption, Photoionization and Photoelectron Spectroscopy*, Academic Press, New York (1979).
103. P. G. Burke and C. J. Joachain (Eds.). *Photon and Electron Collisions with Atoms and Molecules*, Plenum Press, New York (1997).
104. A. J. B. Robertson. *Mass Spectrometry*, Methuen, London (1954).
105. F. H. Field and J. L. Franklin. *Electron Impact Phenomena*, Academic, New York (1957).
106. C. A. McDowell. *Mass Spectrometry*, McGraw-Hill, New York (1963).
107. F. W. McLafferty. *Mass Spectrometry of Organic Molecules*, Academic Press, New York (1963).
108. R. W. Kiser. *Introduction to Mass Spectrometry and Its Applications*, Prentice Hall, Englewood Cliffs, NJ (1965).
109. R. I. Reed (Ed.). *Mass Spectrometry*, Academic Press, London (1965).
110. R. I. Reed (Ed.), *Modern Aspects of Mass Spectrometry*, Plenum Press, New York (1968).
111. E. Illenberger and J. Momigny. *Gaseous Molecular Ions, An Introduction to Elementary Processes Induced by Ionization*, Steinkopff Verlag, Darmstadt and Springer Verlag, New York (1992).
112. E. P. Wigner. *Phys. Rev.* **112**, 1002–1009 (1948).
113. G. H. Wannier. *Phys. Rev.* **90**, 817 (1953); **100**, 817–825 (1956).
114. S. Geltman. *Phys. Rev.* **102**, 171–179 (1956).
115. J. D. Morisson. *J. Appl. Phys.* **28**, 1409–1413 (1957).

116. H. M. Rosenstock and M. Krauss. In *Mass Spectrometry of Organic Ions*, F. W. McLafferty (Ed.), Academic Press, New York (1963).
117. W. Forst. *Theory of Unimolecular Reactions*, Academic Press, New York (1973).
118. Th. Baer and W. L. Hase. *Unimolecular Reaction Dynamics: Theory and Experiment*, Oxford University Press, Oxford (1996).
119. J. Momigny. *Bull. Soc. Chim. Belges* **73**, 357–372 (1964).
120. A. A. Dronin and L. N. Gorokhov. *Teplofiz. Vys. Temp.* **10**, 49–54 (1972).
121. P. Gräber and K. G. Weil. *Ber. Bunsen-Ges. Phys. Chem.* **77**, 507–512 (1973).
122. J. Drowart. In *Proceedings of the 29th Annual Conf. Mass Spectrometry and Allied Topics*, pp. 43–45, ASMS, Minneapolis, MN (1981).
123. J. Drowart. *Pure Appl. Chem.* **56**, 1569–1575 (1984).
124. S. Banon, C. Chatillon, M. Allibert. *High Temp. Sci.* **15**, 17–40 (1982).
125. D. W. Bonnell, J. W. Hastie, K. F. Zmbov. *High Temp. High Press.* **20**, 251–262 (1988).
126. R. P. Burns, G. De Maria, J. Drowart, M. G. Inghram. *J. Chem. Phys.* **38**, 1035–1036 (1963).
127. I. Cornides and T. Gál. *High Temp. Sci.* **14**, 71–76 (1981).
128. H. E. Beske, A. Hurrle, K. P. Jochum. *Fresenius' Z. Anal. Chem.* **309**, 258–261 (1981).
129. J. Van Puymbroeck, R. Gijbels, M. Viczián, I. Cornides. *Int. J. Mass Spectrom. Ion Processes* **56**, 269–280 (1984).
130. Physical stability of a molecular ion is a necessary but insufficient condition for detecting the corresponding neutral molecule after ionization with electrons (or photons). The Franck–Condon principle should, in addition, allow transitions between the bound parts of the respective potential energy curves or surfaces.
131. K. Franzreb, A. Wucher, H. Oechsner. *Phys. Rev. B* **43**, 14396–14399 (1991).
132. K. Franzreb, A. Wucher, H. Oechsner. *Z. Phys. D* **19**, 77–79 (1991).
133. S. M. Younger and T. D. Märk. In *Electron Impact Ionization*, T. D. Märk and G. H. Dunn (Eds.), Chap. 2, pp. 24–41, Springer Verlag, New York (1985).
134. J. W. Otvos and D. P. Stevenson. *J. Am. Chem. Soc.* **78**, 546–551 (1956).
135. M. Gryzinski. *Phys. Rev. A* **2**, 336–358 (1965).
136. S. S. Lin and F. E. Stafford. *J. Chem. Phys.* **48**, 3885–3890 (1968).
137. W. Lotz. *Z. Phys.* **232**, 101–107 (1970).
138. J. B. Mann. *J. Chem. Phys.* **46**, 1646–1651 (1967).
139. J. B. Mann. In *Recent Developments in Mass Spectroscopy, Proceedings of the Conference on Mass Spectroscopy, Tokyo*, K. Ogata and T. Hayakawa, (Eds.), pp. 814–819, University Park Press, Baltimore, MD (1970).
140. J. P. Desclaux. *Atomic Data Nuclear Data Tables* **12**, 311–406 (1973).
141. K. L. Bell, H. B. Gilbody, J. G. Hughes, A. E. Kingston, F. J. Smith. *J. Phys. Chem. Ref. Data* **12**, 891–916 (1983).
142. M. A. Lennon, K. L. Bell, H. B. Gilbody, J. G. Hughes, A. E. Kingston, M. J. Murray, F. J. Smith. *J. Phys. Chem. Ref. Data* **17**, 1285–1363 (1988).
143. D. W. Bonnell and J. W. Hastie. Program SIGMA, a Fortran code for computing atomic ionization cross-sections from data in the fitting formalism of [141]. Detailed tables of calculated [139] cross-sections were kindly made available by Dr. J. B. Mann. Fitting was based on linear regression techniques and graphical comparison of data. Program SIGMA is available on request, together with σ vs. E coefficient data, in IBM PC executable format or as source code. National Institute of Standards and Technology, Gaithersburg, MD, unpublished work (1990–1997).
144. L. J. Kieffer and G. H. Dunn. *Rev. Modern Phys.* **38**, 1–35 (1966).
145. H. Tawara and T. Kato. *Atomic Data Nuclear Data Tables* **36**, 167–353 (1987).
146. R. C. Wetzel, F. A. Baiocchi, T. R. Hayes, R. S. Freund. *Phys. Rev. A* **35**, 559–577 (1987).
147. T. R. Hayes, R. C. Wetzel, R. S. Freund. *Phys. Rev. A* **35**, 578–584 (1987).
148. R. J. Shul, R. C. Wetzel, R. S. Freund. *Phys. Rev. A* **39**, 5588–5596 (1989).

149. R. S. Freund, R. C. Wetzel, R. S. Shul, T. R. Hayes. *Phys. Rev. A* **41**, 3575–3595 (1990).
150. S. Matt, B. Dünser, M. Lezius, H. Deutsch, K. Becker, A. Stamatovic, P. Scheier, T. D. Märk. *J. Chem. Phys.* **105**, 1880–1896 (1996).
151. R. H. G. Reid, K. Bartschat, P. G. Burke. *J. Phys. B: At. Mol. Opt. Phys.* **25**, 3175–3185 (1992).
152. A. N. Nelson. AFML-TR-75-198 (1976).
153. E. G. McGuire. *Phys. Rev.* **20**, 3175–3185 (1992).
154. Y.-K. Kim, J. M. Migdalek, W. Siegal, J. Bieron. *Phys. Rev. A* **57**, 246–254 (1998).
155. K. D. Carlson and E. G. Rauh. *High Temp. Sci.* **16**, 341–357 (1983)
156. M. B. Shah, D. S. Elliott, H. B. Gilbody. *J. Phys. B: At. Mol. Phys.* **20**, 3501–3514 (1987).
157. D. P. Almeida, A. C. Fontes, C. F. L. Godinho. *J. Phys. B: At. Mol. Phys.* **28**, 3335–3345 (1995).
158. A. R. Johnston and P. D. Burrow. *Phys. Rev. A* **51**, R1735–R1737 (1995).
159. P. McCallion, M. B. Shah, H. B. Gilbody. *J. Phys. B: At. Mol. Phys.* **25**, 1061–1071 (1992).
160. P. McCallion, M. B. Shah, H. B. Gilbody. *J. Phys. B: At. Mol. Phys.* **25**, 1051–1060 (1992).
161. H. C. Straub, P. Renault, B. G. Lindsay, K. A. Smith, R. F. Stebbings. *Phys. Rev. A* **52**, 1115–1124 (1995).
162. I. I. Shafranyosh and M. O. Magitich. *J. Phys. B* **33**, 905–910 (2000).
163. M. B. Shah, P. McCallion, K. Okuno, H. B. Gilbody. *J. Phys. B: At. Mol. Phys.* **26**, 2393–2401 (1993).
164. M. A. Bolorizadeh, C. J. Patton, M. B. Shah, H. B. Gilbody. *J. Phys. B: At. Mol. Phys.* **27**, 175–183 (1994).
165. C. J. Patton, K. O. Lozhkin, M. B. Shah, J. Geddes, H. B. Gilbody. *J. Phys. B: At. Mol. Phys.* **29**, 1409–1417 (1996).
166. P. C. E. McCartney, M. B. Shah, J. Geddes, H. B. Gilbody. *J. Phys. B: At. Mol. Phys.* **31**, 4821–4831 (1998).
167. H. Deutsch and T. D. Märk. *Int. J. Mass Spectr. Ion Processes* **79**, R1–R8 (1987).
168. H. Deutsch, D. Margreiter, T. D. Märk. *Z. Phys. D* **29**, 31–37 (1994).
169. D. Margreiter, H. Deutsch, M. Schmidt, T. D. Märk. *Int. J. Mass Spectr. Ion Processes* **100**, 157–176 (1990).
170. A. G. Harrison, E. G. Jones, S. K. Gupta, G. P. Nagy. *Can. J. Chem.* **44**, 1967–1973 (1966).
171. J. A. Beran and L. Kevan. *J. Phys. Chem.* **73**, 3866–3876 (1969).
172. R. Alberti, M. M. Genoni, C. Pascual, J. Vogt. *Int. J. Mass Spectrom. Ion Phys.* **14**, 89–98 (1974).
173. W. L. Fitch and A. D. Sauter. *Anal. Chem.* **55**, 832–835 (1983).
174. H. Deutsch and M. Schmidt. *Contrib. Plasma Phys.* **25** (5), 475–484 (1985).
175. H. Deutsch, P. Scheier, T. D. Märk. *Int. J. Mass Spectr. Ion Processes* **74**, 81–95 (1986).
176. H. Deutsch, D. Margreiter, T. D. Märk. *Int. J. Mass Spectr. Ion Processes* **93**, 259–264 (1989).
177. J. Berkowitz and J. R. Marquart. *J. Chem. Phys.* **37**, 1853–1865 (1962).
178. F. W. Lampe, J. L. Franklin, F. H. Field. *J. Am. Chem. Soc.* **79**, 6129–6132 (1957).
179. D. Margreiter, H. Deutsch, T. D. Märk. *Contrib. Plasma Phys.* **30**, 487–495 (1990).
180. H. Deutsch, C. Cornelissen, L. Cespiva, V. Bonacic-Koutecky, D. Margreiter, T. D. Märk. *Int. J. Mass Spectr. Ion Processes* **129**, 43–48 (1993).
181. H. Deutsch, T. D. Märk, V. Tarnovsky, K. Becker, C. Cornelissen, L. Cespiva, V. Bonacic-Koutecky. *Int. J. Mass Spectr. Ion Processes* **137**, 77–91 (1994).
182. H. Deutsch, K. Becker, T. D. Märk. *Int. J. Mass Spectrom. Ion Processes* **167/169**, 503–517 (1997).
183. M. Bobeldijk, W. J. van der Zande, P. G. Kistemaker. *Chem. Phys.* **179**, 125–130 (1994).
184. Y.-K. Kim and M. E. Rudd. *Phys. Rev. A* **50**, 3954–3967 (1994).
185. W. Hwang, Y.-K. Kim, M. E. Rudd. *J. Chem. Phys.* **104**, 2956–2966 (1996).
186. J. M. Rost and Th. Pattard. *Phys. Rev. A* **55**, R5–R7 (1997).
187. C. Vallance, S. A. Harris, J. E. Hudson, P. W. Harland. *J. Phys. B: At. Mol. Opt. Phys.* **30**, 2465–2475 (1997).

188. L. Pauling. *The Nature of the Chemical Bond and the Structure of Molecules and Crystals: An Introduction to Modern Structural Chemistry*, 3rd ed., Cornell Univ. Press, Cornell, NY (1980).
189. G. Herzberg. *Molecular Spectra and Molecular Structure I. Spectra of Diatomic Molecules*, D. Van Nostrand, New York (1959).
190. C. Younes. Ph.D. thesis. *Contribution à l'étude thermodynamique par spectrometrie de masse à haute température des Oxydes* MO_{2-x}, [M=U, (U,La), (La,Ce), (La,Ce,Y), (U,Ce)], Chap. II, pp. 33–47, Université de Paris-Sud, Centre d'Orsay, order number 3199 (1986).
191. J. W. Hastie, D. W. Bonnell, A. J. Paul, J. Yeheskel, P. K. Schenck. *High Temp. Mat. Sci.* **33**, 135–169 (1995).
192. D. W. Bonnell and J. W. Hastie. "A Theoretical Analysis of Temperature Dependent Electron Impact Fragmentation," *Proceedings of the 31st Annual American Society for Mass Spectrometry Symposium* (1983).
193. E. N. Nicolaev. *Khim. Vys. Energii.* **3**, 49 (1972).
194. R. I. Sheldon and P. W. Gilles. In *Characterization of High Temperature Vapors and Gases NBS SP-561/1,* J. W. Hastie (Ed.), pp. 231–235, NIST, Gaithersburg, MD (1979).
195. M. Sai Baba, T. S. L. Marasimhan, R. Balasubramanian, C. K. Mathews. *Int. J. Mass Spect. Ion Processes* **114**, R1–R8 (1992).
196. M. Sai Baba, T. S. L. Marasimhan, R. Balasubramanian, C. K. Mathews. *Int. J. Mass Spect. Ion Processes* **116**, R1–R6 (1992).
197. A. Popovič. *Rapid. Commun. Mass Spectrom.* **10**, 1433–1438 (1996).
198. D. Detry, J. Drowart, P. Goldfinger, H. Keller, H. Rickert. *Z. Phys. Chem. N. F.* **55**, 314–317 (1967).
199. J. Drowart, P. Goldfinger, D. Detry, H. Rickert, H. Keller. *Adv. Mass Spectrometry* **4**, E. Kendrick (Ed.), pp. 499–509, Institute of Petroleum, London (1968).
200. H. Keller, H. Rickert, D. Detry, J. Drowart, P. Goldfinger. *Z. Phys. Chem. N. F.* **75**, 273–286 (1971).
201. O. Knacke and A. von Richthofen. *Z. Phys. Chem.* **187**, 257–264 (1994).
202. G. De Maria and V. Piacente. *Bull. Soc. Chim. Belges* **81**, 155–162 (1972).
203. V. Piacente, L. Malaspina, G. Bardi. *High Temp. Sci.* **5**, 395–402 (1973).
204. P. Rocabois, C. Chatillon, C. Bernard. *Rev. Int. Hautes Tempér. Réfract., Fr.* **28**, 37–48 (1992–1993).
205. J. Kapala, D. Kath, K. Hilpert. *Metall. Mater. Trans*. **27A**, 2673–2677 (1996).
206. E. J. Rolinski, Ch. J. Oblinger, M. Hoch. *Int. J. Mass Spectrom. Ion Phys.* **5**, 408–412 (1970).
207. C. B. Alcock. *High Temp. High Press.* **20**, 165–168 (1988).
208. G. R. Belton and R. J. Fruehan. *J. Phys. Chem.* **71**, 1403–1409 (1967).
209. R. C. Paule and J. Mandel. *Pure Appl. Chem.* **31**, 371–394 (1972).
210. J. Philippot, O. Pesme, R. Fouilleul, J. J. Laforet, D. Semet, A. Pattoret. In *Adv. Mass Spectrom. 1985*, J. F. J. Todd (Ed.), pp. 1021–1022, John Wiley, New York (1986).
211. J. R. McCreary and R. J. Thorn. *High Temp. Sci.* **4**, 506–516 (1972); *ibid.*, 205–214.
212. R. Kematick, J. Anderegg, H. Franzen. *High Temp. Sci.* **19**, 17–28 (1985).
213. E. Storms, B. Calkin, A. Yencha. *High Temp. Sci.* **1**, 430–455 (1969).
214. A. Buechler and J. L. Stauffer. In *Thermodynamics*, Vol. I, pp. 271–290, IAEA, Vienna (1966).
215. A. Pattoret, S. Smoes, J. Drowart. In *Thermodynamics*, Vol. I, pp. 377–380, IAEA, Vienna (1966).
216. A. Chatillon. *Proc. Electrochem. Soc.* **97-39**, 648–656 (1997).
217. J. V. Hackworth, M. Hoch, H. L. Gegel. *Metall. Trans.* **2**, 1799–1805 (1971).
218. A. Chatillon, M. Allibert, A. Pattoret. *Adv. Mass Spectrom.* **7A**, N. R. Daly (Ed.), pp. 615–621, Institute of Petroleum, London (1978).
219. B. Granier, C. Chatillon, M. Allibert. *High Temp. Sci.* **23**, 115–145 (1987).
220. L. F. Malheiros, C. Chatillon, M. Allibert. *High Temp. High Press.* **25**, 35–51 (1993).
221. L. F. Malheiros, C. Chatillon, M. Allibert. *Rev. Int. Hautes Tempér. Réfrac., Fr.* **29**, 89–99 (1994).

222. M. Allibert, C. Chatillon, K. T. Jacob, R. Lourtau. *J. Am. Ceram. Soc.* **64**, 307–314 (1981).
223. K. Hilpert. *Ber. Bunsen-Ges. Phys. Chem.* **84**, 494–499 (1980).
224. M. Albess, M. Saibaba, D. Kath, M. Miller, K. Hilpert. *Ber. Bunsen-Ges. Phys. Chem.* **96**, 1663–1668 (1992).
225. K. Hilpert, H. Gerads, D. Robertz. *Ber. Bunsen-Ges. Phys. Chem.* **89**, 43–48 (1985).
226. K. Hilpert, K. Ruthardt. *Ber. Bunsen-Ges. Phys. Chem.* **91**, 724–731 (1987).
227. A. Neckel. In *Thermochemistry of Alloys*, H. Brodowsky and H.-J. Schaller (Eds.), pp. 221–246, Kluwer Academic, Boston (1989).
228. J. Tomiska. *CALPHAD* **10**, 91–100 (1986).
229. J. Tomiska and J. Vrestal. *Thermochim. Acta* **314**, 155–167 (1998).
230. E. R. Plante, J. W. Hastie, M. Kowalska. *ISJI Int.* **32** (12), 1276–1279 (1992).
231. I. Prigogine, R. Defay, translated by D. H. Everett. *Chemical Thermodynamics*, Longmans, London (1965).
232. R. S. Swalin. *Thermodynamics of Solids*, 2nd ed., John Wiley, New York (1972).
233. C. H. P. Lupis. *Chemical Thermodynamics of Materials*, Elsevier Science, New York (1983).
234. G. N. Lewis and M. Randall, revised by K. S. Pitzer and L. Brewer. *Thermodynamics*, 3rd ed., McGraw-Hill, New York (1995).
235. D. R. Gaskell. *Introduction to the Thermodynamics of Materials*, Taylor & Francis, New York (2003).
236. J. E. Mayer and M. Goepert-Mayer. *Statistical Mechanics*, John Wiley, New York (1950).
237. G. Herzberg. *Molecular Spectra and Molecular Structure II. Infrared and Raman Spectra of Polyatomic Molecules*, D. Van Nostrand, New York (1945).
238. D. R. Stull and H. Prophet. In *The Characterization of High Temperature Vapors*, J. L. Margrave (Ed.), pp. 359–424, John Wiley, New York (1967).
239. G. Herzberg. *Molecular Spectra and Molecular Structure III. Electronic Spectra and Electronic Structure of Polyatomic Molecules*, D. Van Nostrand, New York (1966).
240. C. W. Bauschlicher, Jr. and S. R. Langhof. *J. Chem. Phys.* **87**, 2919–2924 (1987).
241. C. W. Bauschlicher, Jr. and H. Partridge. *J. Chem. Phys.* **109**, 4707–4712 (1998).
242. Dingguo Dae and K. Balasubramanian. *J. Chem. Phys.* **108**, 4379–4385 (1998).
243. G. Igel-Man, H. Stoll, H. Preuss. *Mol. Phys.* **80**, 325–339 (1993); *ibid.* 341–354 (1993).
244. I. Shim, M. Sai Baba, K. A. Gingerich. *J. Phys. Chem. A* **109**, 10763–10767 (1998).
245. O. Kubaschewski, C. B. Alcock, P. J. Spencer. *Metallurgical Thermochemistry*, Pergamon Press, Oxford (1993).
246. R. M. Badger. *J. Chem. Phys.* **2**, 128–131 (1934); *ibid.* **3**, 710–714 (1935).
247. W. Gordy. *J. Chem. Phys.* **14**, 305–320 (1946).
248. K. M. Guggenheimer. *Proc. Phys. Soc. London* **58**, 456–468 (1946).
249. E. B. Wilson, Jr., J. C. Decius, P. C. Cross. *Molecular Vibrations. The Theory of Infrared and Raman Vibrational Spectra*, Dover, New York (1980).
250. D. J. Frurip and M. Blander. In *Characterization of High Temperature Vapors and Gases* **NBS SP-561/2**, J. W. Hastie (Ed.), pp. 1597–1609, NIST, Gaithersburg, MD (1979); *J. Chem. Phys.* **73**, 509–518 (1980).
251. D. J. Frurip, C. Chatillon, M. Blander. *J. Chem. Phys.* **86**, 647–653 (1982).
252. D. J. Frurip, M. Blander, C. Chatillon. In *Metal Bonding and Interactions in High Temperature Systems, with Emphasis on Alkali Metals*, J. L. Gole and W. C. Stwalley (Eds.), pp. 207–218, ACS Symposium Series 179, American Chemical Society, Washington, DC (1982).
253. S. Smoes and J. Drowart. *Faraday Symp. Chem. Soc.* **8**, 139–148 (1973).
254. IUPAC. *Quantities, Units and Symbols in Physical Chemistry,* 2nd ed. Prepared for publication by I. Mills, T. Cvitaš, K. Homann, N. Kallay, K. Kuchitsu. Blackwell Science, Oxford, UK (1993).
255. D. H. Whiffen. *Pure Appl. Chem.* **51**, 1–36 (1979).
256. W. L. Winterbottom. *J. Chem. Phys.* **47**, 3546–3556 (1967).

257. R. J. Thorn. *J. Chem. Phys.* **52**, 474–476 (1970).
258. E. R. Plante and R. C. Paule. *J. Chem. Phys.* **53**, 3770–3771 (1970).
259. J. R. McCreary and R. J. Thorn. *J. Chem. Phys.* **53**, 3771–3772 (1970).
260. J. R. McCreary and R. J. Thorn. *High Temp. Sci.* **5**, 97–112 (1970).
261. A. Garvin, T. Golashvili, H.V. Kehaian, N. Kurti, E. F. Westrum, Jr. *CODATA Bull.* **9** (1973).
262. G. Olofsson. *J. Chem. Thermodyn.* **13**, 603–622 (1981); *Pure Appl. Chem.* **53**, 1805–1825 (1981).
263. G. Olofsson. In *Combustion Calorimetry*, S. Sunner and M. Månsson (Eds.), pp. 137–159, Pergamon Press, Oxford (1979).
264. V. A. Medvedev. In *Combustion Calorimetry*, S. Sunner and M. Månsson (Eds.), pp. 161–162, Pergamon Press, Oxford (1979).
265. F. D. Rossini. *Experimental Thermochemistry*, pp. 297–320, Wiley Interscience, New York (1956).
266. R. Hultgren, R. L. Orr, P. D. Anderson, K. K. Kelley. *Selected Values of Thermodynamic Properties of Metals and Alloys*, p. V, John Wiley, New York (1963).
267. A. Kant. Private communication.
268. L. H. Rovner and J. H. Norman. *J. Chem. Phys.* **52**, 2946–2929 (1970).
269. A. W. Searcy, W. S. Williams, P. O. Schissel. *J. Chem. Phys.* **32**, 957–958 (1960).
270. Laboratorium Fysische Chemie, Vrije Universiteit Brussel. Unpublished.
271. S. Smoes, W. R. Pattje, J. Drowart. *High Temp. Sci.* **10**, 109–130 (1978).
272. J. Drowart and S. Smoes. In *Thermochemical Data Acquisition, Part II*, EUR 14844 EN. Commission of the European Communities (1992).
273. K. Hilpert and M. Miller. Private communication.
274. R. S. Freund, R. C. Wetzel, R. J. Shul. *Phys. Rev. A* **41**, 5861–5868 (1990).
275. A. Vande Gucht. Ph.D. thesis, Vrije Universiteit Brussel (1990).
276. R. I. Ackerman, E. G. Rauh, C. A. Alexander. *High Temp. Science* **7**, 304–316 (1975).
277. L. N. Gorokhov and N. E. Khandamirova. *Adv. Mass Spec.* **13**, 1031–1032 (1985).
278. P. E. Blackburn and P. M. Danielson. *J. Chem. Phys.* **56**, 6156–6164 (1972).
279. R. J. Shul, R. S. Freund, R. S. Wetzel. *Phys. Rev. A* **41**, 5856–5860 (1990).
280. D. R. Hayes, R. C. Wetzel, F. A. Baiocchi, R. S. Freund. *J. Chem. Phys.* **88**, 823–829 (1988).
281. G. Monnom, Ph. Gaucherel, C. Paparoditis. *J. Physique* **45**, 77–84 (1984).
282. T. Petric and C. Chatillon. Unpublished.
283. R. Colin and J. Drowart. *Trans. Faraday Soc*. **64**, 2611–2621 (1969).
284. R. J. Shul, T. R. Hayes, R. C. Wetzel, F. A. Baiocchi, R. S. Freund. *J. Chem. Phys.* **89**, 4042–4047 (1988).
285. T. R. Hayes, R. J. Shul, F. A. Baiocchi, R. C. Wetzel, R. S. Freund. *J. Chem. Phys.* **89**, 4035–4041 (1988).
286. L. N. Sidorov and V. B. Shol'ts. *Int. J. Mass. Spectrom. Ion Phys.* **8**, 437–458 (1972).
287. V. E. Shevchenko, M. K. Iljin, O. T. Nikitin, L. N. Sidorov. *Int. J. Mass. Spectrom. Ion Phys.* **21**, 279–295 (1976).